International Journal of Nanomedicine

Dovepress
open access to scientific and medical research

Open Access Full Text Article

ORIGINAL RESEARCH

Long-Circulating Lipid Nanospheres Loaded with Flurbiprofen Axetil for Targeted Rheumatoid Arthritis Treatment

Zhenyu Chen[1,2,*], Zhongbing Liu[1,*], Shuzao Wang[1,*], Cai Cheng[1,*], Xiaoduan Sun[1], Zerong Liu[3], Jun Wei[1], Jun Jiang[4,5], Huaqi Lan[1], Meiling Zhou[6], Pei Jing[6], Yan Lin[1], Xiangyu Zhou[7], Zhirong Zhong[1,3,8]

[1]Key Laboratory of Medical Electrophysiology, Ministry of Education, School of Pharmacy, Southwest Medical University, Luzhou, Sichuan, 646000, People's Republic of China; [2]The Second People's Hospital of China Three Gorges University, Yichang, 443000, People's Republic of China; [3]Central Nervous System Drug Key Laboratory of Sichuan Province, Luzhou, Sichuan, 646000, People's Republic of China; [4]Department of General Surgery (Thyroid Surgery), the Affiliated Hospital of Southwest Medical University, Luzhou, Sichuan, 646000, People's Republic of China; [5]Metabolic Vascular Diseases Key Laboratory of Sichuan Province, Luzhou, Sichuan, 646000, People's Republic of China; [6]Department of Pharmacy, The Affiliated Hospital of Southwest Medical University, Luzhou, Sichuan, 646000, People's Republic of China; [7]Department of Thyroid and Vascular Surgery, the Affiliated Hospital of Southwest Medical University, Luzhou, Sichuan, 646000, People's Republic of China; [8]Key Laboratory of Luzhou City for Aging Medicine, Department of Pharmacology, School of Pharmacy, Southwest Medical University, Luzhou, Sichuan, 646000, People's Republic of China

*These authors contributed equally to this work

Correspondence: Xiangyu Zhou; Zhirong Zhong, Email xiangyuzhou971@vip.126.com; zhongzhirong@126.com

Background: Flurbiprofen axetil (FA) is a non-steroidal anti-inflammatory drug with good analgesic and anti-inflammatory effects. However, it suffers from poor solubility, short circulation time, and off-target binding profile, which significantly limit its clinical application. Here, we loaded FA into stealth lipid microspheres modified with the arginine-glycine-aspartic acid (RGD) peptide (cRGD-FA-SLM), and examined the therapeutic potential of the resulting platform for the treatment of rheumatoid arthritis (RA).

Methods: cRGD-FA-SLM was prepared by high pressure homogenization, and its toxicity and uptake by macrophages were examined using cultures of RAW264.7 cells. Hemolysis and hepatotoxicity tests were performed to assess the safety of the developed platform, while its pharmacokinetics, biodistribution, and therapeutic efficacy were investigated in a collagen-induced arthritis rat model.

Results: cRGD-FA-SLM showed homogeneous spherical morphology and efficient encapsulation of FA. The developed platform was non-toxic to normal macrophages and was selectively internalized by lipopolysaccharide-activated macrophages in vitro, while it distributed mainly to arthritic joints and significantly prolonged FA in circulation in vivo. cRGD-FA-SLM also significantly reduced the expression of prostaglandin E2 and alleviated joint edema and bone erosion, showing prolonged analgesic effects in arthritic rats.

Conclusion: cRGD-FA-SLM shows good inflammation-targeting ability and prolongs drug circulation in vivo, suggesting promise as an anti-inflammatory and analgesic agent for targeted RA treatment.

Keywords: flurbiprofen axetil, lipid nanospheres, cRGD, long circulation, rheumatoid arthritis

Introduction

Rheumatoid arthritis (RA) is an autoimmune disease characterized by systemic symmetry and chronic inflammation of the joints.[1] Chronic synovitis, synovial cell hyperplasia, and vascular opacification predominate at the site of inflammation,[2,3] but how genetics, infections or other factors contribute to the disease is unclear.[4]

The current first-line treatment against RA is non-steroidal anti-inflammatory drugs (NSAIDs) such as flurbiprofen axetil (FA), glucocorticoids, disease-modifying anti-rheumatic drugs, and biologic anti-rheumatic drugs.[5,6] These drugs are quite effective at relieving pain, inflammation and stiffness in RA, delaying disease progression, maintaining joint function and reducing disability.[7] In fact, NSAIDs show stronger anti-inflammatory and analgesic effects than many

Received: 17 May 2023
Accepted: 9 August 2023
Published: 8 September 2023

Graphical Abstract

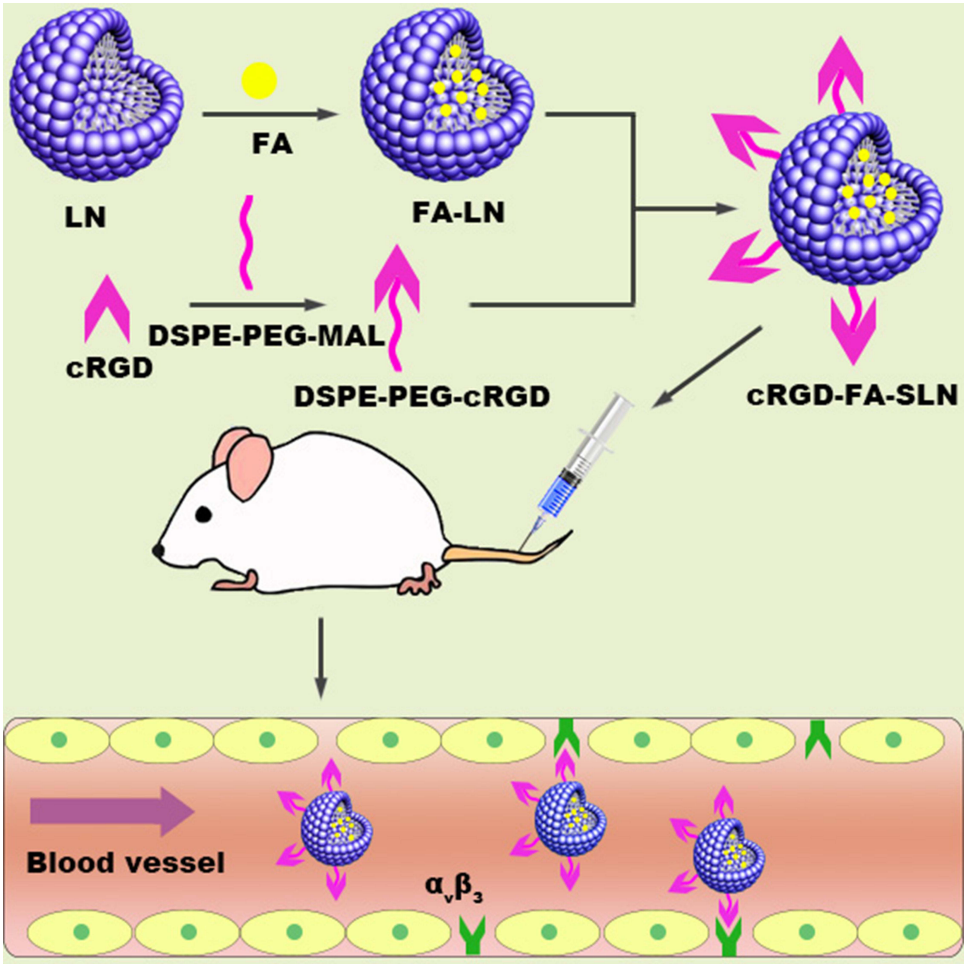

other RA treatments.[8] However, NSAIDs do not specifically target inflamed tissue, increasing risk of adverse systemic effects such as gastrointestinal toxicities, cardiovascular risks, renal injuries, and hepatotoxicity as well as hypertension and other minor disorders. Although there are various distinctive treatment methods for RA,[9,10] highly specific treatments against RA have yet to be described,[11] highlighting the need for safe drug delivery systems that can target affected joints.

During RA, highly permeable neovascular lesions with distorted structures form at sites of inflammation, promoting extravasation through the effect of leaky vasculature and subsequent inflammatory cell-mediated sequestration (ELVIS), similar to the enhanced permeability and retention (EPR) effect in tumor cells. This may serve as the basis for targeting drug delivery systems to sites of inflammation.[12,13] RAW264.7 macrophages are the most commonly used cells in the study of RA.[14–16] It has also been found that $\alpha_v\beta_3$ integrin is overexpressed in neovascular lesions and in activated macrophages during RA.[17,18] Therefore, we hypothesized that $\alpha_v\beta_3$ would serve as an important binding site for selective drug delivery and active targeting of the inflammation site, enhancing therapeutic effects while reducing necessary drug doses and thereby the associated toxicity. Short peptides containing arginine-glycine-aspartic acid (RGD) can act as recognition sites that can bind to integrin $\alpha_v\beta_3$ overexpressed in neovascularization sites.[19] However, only cyclic RGD-containing peptides (cRGD) are resistant to chemical degradation.[19]

FA has been found to downregulate prostaglandin E2 (PGE2), leading to stronger anti-inflammatory and analgesic effects at the inflammation site than with conventional NSAIDs.[20,21] Lipid nanospheres (LNs) can also effectively target inflammatory or tumor sites through the EPR effect, offering sustained drug release and prolonged time in circulation,

while reducing the gastrointestinal side effects of oral administration.[22] However, lipophilic carriers are efficiently captured by the reticuloendothelial system (RES) and quickly cleared by systemic circulation, leading to low accumulation at the target site.[23] It was reported that the coat of polyethylene glycol (PEG) on the surface of a preparation is not recognized by the RES, while the long, hydrophilic PEG chains significantly improve drug pharmacokinetics and enhance the EPR effect.[24]

However, either PEGylation or conjugation of targeting ligand on their own can improve pharmacokinetics or pharmacodynamics of nanomedicines only to a certain extent. For example, PEGylation of nanomedicines prolongs their half-life in plasma, but often blocks interactions between the nanomaterials and target tissue. Similarly, conjugation of targeting ligand to the surface of nanomedicines improves their ability to target tissue and be internalized through receptor-mediated endocytosis, but the modified nanomedicines remain susceptible to opsonization by RES. Therefore, combining PEGylation and conjugation with targeting ligand together, known as "multi-functionalization", has become a promising direction for formulating advanced nanomedicines.[25]

In this study, we prepared FA-loaded cRGD-modified stealth LNs (hereinafter, cRGD-FA-SLN) as a novel drug delivery system for targeted RA treatment. The developed platform showed an active dual-targeting effect due to the ELVIS effect and the integrin-binding RGD motif, while it successfully avoided RES elimination, improving the delivery and therapeutic efficacy of FA and reducing the necessary dosage with its associated toxicity.

Materials and Methods

Materials

Flurbiprofen and FA were obtained from Beijing Solarbio Biotechnology (Beijing, China). cRGD was purchased from Nanjing Peptide Industry Biotechnology (Nanjing, China), while DSPE-PEG_{2000}-Mal (DSPE, distearoyl phosphatidyl ethanolamine; Mal, maleimide), DSPE-PEG_{2000}, and coumarin-6 were from Xi'an Ruixi Biotechnology (Xi'an, China). Lecithin was provided by Guangzhou Baiyun Mountain Hanfang Modern Co. Ltd. (Guangzhou, China), and soybean oil was from Aladdin Co. Ltd. (Shanghai, China). 3-(4,5-Dimethyl-2-thiazolyl)-2,5-diphenyl-2*H*-tetrazolium bromide (MTT) and 4',6-diamidino-2-phenylin-dole dihydrochloride (DAPI) were purchased from Biyuntian Biotechnology (Shanghai, China), while Dulbecco's modified Eagle medium, fetal bovine serum, and penicillin/streptomycin were from Gibco-BRL (New York, America). 1.1-Dioctadecyl-3,3,3,3-tetramethylindotricarbocyanine (DiR) iodide was obtained from Lambolide Biotechnology Co., Ltd. (Beijing, China). Bovine type II collagen and Freund's adjuvant (complete and incomplete) were purchased from Chondrex (Beijing, China). All other reagents were obtained from Kelong Company (Chengdu, China). The enzyme-linked immunosorbent assay (ELISA) against PGE2 was obtained from Andy Gene Biotechnology (Beijing, China), and RAW 264.7 cells were purchased from the American Type Culture Collection (Manassas, VA, USA) and cultured in the Pharmacy Laboratory of Southwest Medical University. Adult male Sprague-Dawley rats were supplied by Chengdu Dasuo Biological Technology (Chengdu, China; certificate no. 211002300058522). Since we expected the pharmacokinetics of FA in vivo to be similar between rats of either sex, we used animals of only one sex for simplicity. All animal experiments were performed strictly in accordance with institutional guidelines and protocols approved by the Committee for Animal Experiments of Southwest Medical University [approval no. SYXK (Sichuan) 2018–065].

Collagen-Induced Arthritis Rat Model

For the establishment of the collagen-induced arthritis (CIA) rat model, adult male rats that had been habituated for at least one week in the specific pathogen-free animal room were injected subcutaneously two times with an interval of one week at the base of the tail with an emulsion (100 μL) of bovine type II collagen and complete Freund's adjuvant.[26,27] At 15 days post-injection, CIA severity of hind paws was scored according to the following articular index (AI): 0, no erythema or swelling; 1, minor erythema or swelling; 2, moderate edema and signs extending to the tarsals; 3, significant edema, restricted joint utilization, and signs extending to the metatarsals; or 4, serious signs and excessive edema with joint rigidity extending to the entire hind paw.[28,29] The scores of each paw were summed to calculate the total AI score for each animal.

Optimization of FA-SLN Preparation and Formulation

FA-SLN was prepared by high-pressure homogenization.[30] To prepare the oil phase, FA, poloxamer-188, and DSPE-PEG_{2000} were dissolved in soybean oil and stirred at 65 °C. To prepare the water phase, glycerin, lecithin, disodium hydrogen phosphate and oleic acid were dissolved in water and stirred at 65 °C. The oil phase was then added slowly to the water phase, and colostrum was prepared by high-shear mixing. The mixture was then allowed to cool to room temperature, and the final emulsion was obtained by high-pressure homogenization. FA-SLN formed after adjusting the pH of the emulsion. The formulation of FA-SLN was optimized using the central combination design (CCD) method and considering three variables: soybean oil ratio (X_1), lecithin ratio (X_2), and homogeneous pressure (X_3). These three variables were treated as primary factors affecting the mean size (Y_1) and encapsulation efficiency (Y_2) of the drug-loaded nanospheres. The total number of CCD points was determined to be 15 according to the formula $N = 2^f + 2f + 1$, where f represents the number of factors. The central point was repeated five times to ensure a robust result. The results were analyzed using response surface plots and contour maps obtained with Design-Expert 8.0.6 software.[31]

Synthesis of DSPE-PEG_{2000}-cRGD

To prepare DSPE-PEG_{2000}-cRGD, cRGD and DSPE-PEG_{2000}-Mal were mixed in methanol in a 2:1 molar ratio (Figure S1). DSPE-PEG_{2000}-cRGD was then purified by dialysis in a dialysis bag with a molecular weight cutoff of 3.0 kDa at 37 °C for 24 h,[32,33] dried in vacuo, and analyzed by ^{1}H NMR and Fourier-transform infrared (FTIR) spectroscopy (IRAffinity-1S, Shimadzu, Japan).

Preparation and Characterization of cRGD-FA-SLN

The cRGD-FA-SLN platform was synthesized following the same process as for FA-SLN but using DSPE-PEG_{2000}-cRGD instead of DSPE-PEG_{2000}. The particle size, polydispersity index (PDI), and zeta potential were determined by the dynamic light scattering (DLS) analysis using a Zetasizer Nano ZS90 (Malvern Instruments, Melvin, UK). The sample for DLS measurement was diluted 1:1 (v/v) with phosphate-buffered saline (PBS) to a final volume of 1 mL. The morphologies of LNs, SLN, FA-SLN, and cRGD-FA-SLN were observed by transmission electron microscopy (TEM).[34] To determine the amount of FA in the water phase (M_{water}), 2 mL of sample was added to an ultrafiltration centrifuge tube and centrifuged at 1780 *g* for 30 min. Then, 0.5 mL of the lower filtrate was collected and added to 5 mL of anhydrous ethanol. Another sample was also prepared and ultrasonicated for 5 min to disrupt the emulsion, after which the total amount of FA (M_{total}) was quantified using high-performance liquid chromatography (HPLC) on a reverse-phase C_8 column (Waters XBridge-C_8, 4.6×250 mm, 5.0 μm) with the following conditions: mobile phase, acetic acid/acetonitrile (45:55, v/v); detection wavelength, 254 nm; flow rate, 2.0 mL/min; column temperature, 35 °C; and injection volume, 10 μL. The chromatographic conditions were validated with respect to specificity, linearity, precision, and blank recovery. Encapsulation efficiency (EE) was calculated using the formula: $(\%) = [1 - (\mathrm{Mwater}/\mathrm{Mtotal}]] \times 100$. To assess the stability of FA-SLN and cRGD-FA-SLN, three batches of each formulation were stored at 30 °C for 10 days and at 4 °C for 10 days or three months. Changes in the appearance, centrifugal stability constant (K_e), particle size, and PDI were assessed at 0, 5, and 10 days and at 0, 1, 2, and 3 months.

Lipid Nanosphere Uptake by Cells

FA-LN, FA-SLN, and cRGD-FA-SLN fluorescently labeled were prepared by encapsulating coumarin-6 (100 ng/mL) into LN, and their uptake by RAW264.7 cells, previously activated or not with lipopolysaccharide (LPS), was examined. RAW264.7 cells (1 mL, 3×10^5 cells/mL) were first seeded in a 24-well culture plate and incubated for 2 h. Cells were cultured in serum-free medium to avoid potential interference from proteins in the serum. Cells in the LPS-activated group were incubated with LPS (100 ng/mL) for another 24 h and allowed to differentiate into M1-type cells.[35] Non-activated cells were used as a control. After 24 h, the culture medium was aspirated, then the cells were washed with PBS and incubated for 2 h with 100 μL of fluorescently labeled FA-LN, FA-SLN, or cRGD-FA-SLN and 900 μL of serum- and antibody-free culture medium. The solution was aspirated, then the cells were washed with PBS and fixed with 4% paraformaldehyde for 15 min. Again, the solution was aspirated and the cells were washed with PBS, then the cells were stained with DAPI for 5 min. The staining solution was removed, and the cells were washed with PBS, collected with

forceps, sealed with 50% glycerol, and observed with a confocal laser microscope at 477 nm. The uptake of the prepared formulations by quiescent or activated M1-type macrophages was also examined by fluorescence-activated cell sorting (FACS). Three groups of RAW264.7 cells treated with FA-LN, FA-SLN, or cRGD-FA-SLN were prepared as described above. After incubation for 2 h with the indicated treatment, the solution was aspirated, and 500 μL of trypsin digest was added to each well. After 1 min, culture medium was added to terminate trypsinization, and the resulting cell suspension was aspirated and centrifuged at 700 ×*g* for 4 min. The supernatant was then discarded, and the cells were resuspended in PBS. The centrifugation/resuspension process was repeated twice. After the final centrifugation, the supernatant was discarded, and the cells were resuspended well with PBS, then analyzed by FACS. Quiescent cells served as the control and cells treated with unlabeled formulations as the blank.

Safety Assay

To access the cytotoxicity of the formulations, a suspension of RAW264.7 cells (2×10^4 cells/mL, 100 μL) was seeded in 96-well plates and incubated at 5% CO_2 for 24 h. Afterward, 100 μL of FA, LNs, SLN, FA-LN, FA-SLN, or cRGD-FA-SLN was added at different FA concentrations (5, 20, 60, 120, 240 μg/mL),[36] and cells were incubated for 24, 48, and 72 h. The cells were then washed with PBS, and fresh medium containing 10% MTT was added. After incubation for 4 h, the solution was aspirated, and 150 μL of DMSO was added to each well, followed by shaking at 37 °C for 10 min. Cells cultured in pure medium served as a negative control. Cell viability was determined by measuring the absor bance at 545 nm with a multimodal microplate reader and was calculated according to the formula: $\text{Cell viability } (\%) = \left(A_{sample} - A_{blank}\right) / \left(A_{control} - A_{blank}\right) \times 100$. The hemolytic potential of cRGD-FA-SLN was evaluated in vitro using red blood cells. Briefly, whole blood was collected from normal rats and centrifuged at 500 *g* for 10 min. The supernatant was then discarded, and the remaining suspension was stirred and centrifuged again under the same conditions. This process was repeated multiple times, until a colorless supernatant was obtained. After the supernatant was discarded, saline was added to the centrifuge tube to dilute the erythrocyte suspension to a concentration of 2% (v/v). FA, SLN, FA-LN, FA-SLN, or cRGD-FA-SLN was then added at different FA concentrations (5, 60, or 240 μg/mL), and each mixture was incubated in a water bath at 37 °C for 3 h. The samples were subsequently centrifuged at 700 *g* for 10 min, and 100 μL of the resulting supernatant was added to a 96-well plate. Saline was used as the negative control and ultrapure water as the positive control. The hemolysis rate was determined by measuring the absorbance (A) at 545 nm with a multimodal microplate reader (BioTek Synergy H1, Burlington, VT, USA) and was calculated according to the formula: $\text{Hemolysis rate}(\%) = (\text{Asample} - \text{Anegative control}) / (\text{Apositive control} - \text{Anegative control}) \times 100$.

Release Profile Detection in vivo

Since FA is rapidly degraded to flurbiprofen in vivo, the pharmacokinetics of FA were assessed by measuring the content of flurbiprofen by HPLC. CIA rats were divided into three groups (n = 5) and injected via the tail vein with FA, FA-LN, FA-SLN, or cRGD-FA-SLN (FA, 1.0 mg/kg). Healthy rats were used as negative controls. At 5, 10, 30, 60, 120, 240, 480, and 720 min post-administration, blood samples were collected from the heart of all rats, heparinized, and centrifuged at 700 *g* for 3 min. A 100-μL aliquot of each plasma sample was then mixed with 1 mL of acetonitrile in a 1.5 mL tube, and the resulting mixtures were vortexed for 5 min and centrifuged at 5000 *g* for 15 min. The content of flurbiprofen in the supernatant was measured by HPLC, and the pharmacokinetics were assessed using the non-compartmental technique in the Drug Analysis System 2.1.1 software (Drug Clinical Research Center, Shanghai University of Traditional Chinese Medicine, Shanghai, China).

Biodistribution

Rats treated as described above were sacrificed at 10 min, 4 h, and 8 h post-injection, and their blood, heart, spleen, liver, kidneys, lung, and entire hind limbs were sampled promptly (n = 5 per group). Tissue homogenates were diluted 2:1 (w/w) with saline and centrifuged. Flurbiprofen in the supernatant was assayed using HPLC. DiR-labelled nanospheres were prepared in the same way as the FA-encapsulated nanospheres, except that DiR instead of FA was dissolved in soybean oil when preparing the oil phase. The biodistribution of each formulation in the respective

organs was observed using an AniView100 multi-mode animal in vivo imaging system (Herbstrom, Guangzhou, China). CIA rats were injected (25 μg/kg) via the tail vein with FA-LN, FA-SLN, or cRGD-FA-SLN that had been labeled with DiR (5 μg/mL). Fluorescent signals were measured at 10 min, 4 h, and 8 h post-injection with a small animal imager. All images were normalized to the same range of fluorescence intensity. At the end of the experiment, all animals were sacrificed, and their liver, heart, spleen, lung, kidneys, and entire hind limbs were collected. Fluorescence was measured ex vivo using a multi-mode animal in vivo imaging system. Rats treated with free DiR served as controls, while untreated rats served as the blank.

Weight, Ankle Diameter, Paw Volume, and AI Score

On day 16 after CIA induction, rats were randomly divided into seven groups (n = 5) and injected via the tail vein with saline, SLN, FA, FA-LN, FA-SLN, or cRGD-FA-SLN (FA, 1.0 mg/kg) every three days for 7 times. Healthy rats were used as the control. After each injection, the rats were weighed and the AI score of each leg was evaluated. The ankle diameter from the medial to lateral section was also measured using a digital caliper, and the paw volume was determined with custom-made equipment.

Micro-Computed Tomography (Micro-CT) of Ankle Joints

The effect of the formulations on the quality of ankle joint bones was examined by micro-CT. CIA rats (n = 5) treated with saline, SLN, FA, FA-LN, FA-SLN, or cRGD-FA-SLN were euthanized on day 34 after the first injection, and their hind limbs were collected and fixed in formalin overnight. The muscles were then removed and the following ankle joint characteristics were assessed using a Skyscan 1276 system (Bruker, Billerica, MA, USA): bone mineral density, ratio of bone volume to tissue volume, ratio of bone surface area to bone volume, trabecular number, trabecular thickness, and trabecular spacing.[37,38] Data were processed and analyzed using 3D reconstructions created with the built-in Bruker micro-CT software.

Histological Evaluation of Joint Tissues

After micro-CT scanning, the ankle joint samples were soaked in 15% neutral EDTA. Decalcification was considered complete when there was no resistance to needle puncture. The samples were then embedded in paraffin and stained with hematoxylin–eosin (H&E) and safranin O for histopathological examination.[39] The pathological changes in the synovial joints at the cellular or tissue level were rated according to a four-point scale: 0, no cell infiltration or proliferation; 1, minimal cell infiltration and proliferation; 2, moderate cell infiltration and proliferation; or 3, extensive infiltration and proliferation.[40]

Hepatotoxicity of Drugs and Serum Levels of PGE2

On day 34 after the first injection of immune reagents, blood was collected from rats using a heparin-free sodium collection tube, centrifuged at 1200 × g for 10 min, and the supernatant serum was collected and analyzed for alanine aminotransferase (ALT) and aspartate aminotransferase (AST) in the serum using an automated biochemical analysis tester. Quantitative analysis of PGE2 in rat serum by enzyme-linked immunoassay (ELISA) using specificity of antigen-antibody binding. The thymus and spleen of each group of experimental rats were taken, and the equations for the spleen and thymus coefficients were as follows:

$$\text{Spleen factor}\,(\%) = \text{Spleen mass}\,(\text{mg})/\text{weight}\,(\text{g}) \times 100$$

$$\text{Thymus coefficient}(\%) = \text{Thymusmass}(\text{mg})/\text{weight}(\text{g}) \times 100$$

Analgesic Effect

CIA rats were divided into four groups (n = 5) and injected via the tail vein with saline, FA-SLN, or cRGD-FA-SLN (FA, 1.0 mg/kg) for three days. Each rat was then placed on the cover plate of a full water bath preheated at 55 °C, and the pain threshold, defined as the time between animal placement on the hot plate and the first foot lick, was recorded at 15,

30, and 60 min after the last administration. The pain threshold of each animal was measured three times with an interval of 2 min.[41] Data were considered invalid if the rat jumped more than once during measurement. CIA rats treated as described above were also intraperitoneally administered with saline, FA-SLN, or cRGD-FA-SLN (FA, 1.0 mg/kg) for three consecutive days. Acetic acid solution (0.2 mL / 10 g) was injected at 1 h after the last dose. The number of torsions, defined as contraction of the abdomen inward and extension of the limbs,[42] was recorded at 1 h after the last dose of the formulation and within 15 min after the first 5 min of acetic acid injection.

Statistical Analysis

Statistical analysis was performed using GraphPad Prism 7.0 (GraphPad Software, La Jolla, CA, USA). Differences among groups were assessed using one- or two-way analysis of variance. Data are shown as mean ± standard deviation (SD). Differences associated with $P < 0.05$ were considered statistically significant.

Results

Optimized Formulation

The optimal formulation of the developed platform was identified by CCD screening. Briefly, the following six variables were initially screened as potential factors affecting the EE of FA-SLN: poloxamer ratio, soybean oil ratio, lecithin ratio, cut time, homogeneous number, and homogeneous pressure. The results indicated that the highest EE could be achieved when the poloxamer ratio was 0.15%, the cut time was 6 min, and the homogeneous number was 6 (Figure 1). However, the optimum values of soybean oil ratio (X_1), lecithin ratio (X_2), and homogeneous pressure (X_3) required further investigation, as their effect on EE was much greater than that of the other three factors.

The levels of X_1, X_2 and X_3 and the experimental values of CCD were used to determine the optimal formulation (Tables S1 and S2). The regression equations were as follows:$Y_1 = 236.77 - 17.99X_1 + 7.71X_2 - 12.33X_3 + 1.43X_1X_2 + 0.54X_1X_3 + 2.72X_2X_3 + 22.07X_1^2 + 22.68X_2^2 + 16.83X_3^2 \left(P0.01, R^2 = 0.8366\right)$, and $Y_2 = 95.77 + 2.60X_1 + 3.80X_2 + 1.32X_3 - 2.17X_1X_2 - 1.12X_1X_3 + 1.10X_2X_3 - 3.44X_1^2 - 5.24X_2^2 - 2.75X_3^2 \left(P0.01, R^2 = 0.9267\right)$.

The relationship between independent and dependent variables was assessed using three-dimensional response surface diagrams and contour plots (Figure 2). The response model was mapped against two experimental factors, and the third was kept constant at its middle level. The results indicated that the interaction between X_1 and X_2 had the most significant effect on particle size (Y_1), followed by the interaction between X_2 and X_3 (Figure 2A–C). Similarly, the interaction between X_1 and X_3 had the greatest effect on the EE (Y_2) (Figure 2D–F). Thus, the optimal predicted values for the preparation of FA-SLN with good mean size and high EE were as follows: $X_1 = 11.24\%$, $X_2 = 1.32\%$, and $X_3 = 103.29$ MPa. To verify the optimized formulation, these values were used to construct the FA-SLN platform. The measured values of Y_1, Y_2, and Y_3 were in good agreement with the predicted ones (Table S3), confirming the reliability of the optimization process.

Preparation of DSPE-PEG$_{2000}$-cRGD

The successful preparation of DSPE-PEG$_{2000}$-cRGD was determined by ^{1}H NMR (Figure S2) and FTIR spectroscopy (Figure 3). Specifically, the chemical shift of 7.0 ppm for the hydrogen on the double bond in the maleimide group was not detected in the spectrum of DSPE-PEG$_{2000}$-cRGD, indicating successful Michael addition (Figure S2). In addition, no differences were observed among the FTIR spectra of DSPE-PEG$_{2000}$-Mal, cRGD, and DSPE-PEG-Mal+cRGD, while the characteristic absorption peak at 1708 cm^{-1} for the carbonyl in the maleimide group shifted to 1670 cm^{-1} in the spectrum of DSPE-PEG$_{2000}$-cRGD, confirming successful reaction (Figure 3).

Characterization of LN Formulations

The DLS analysis indicated that the cRGD-FA-SLN particles were homogeneous with an almost neutral surface charge (Figure 4A and Table S4). The TEM analysis also showed that the prepared LN formulations had a regular morphology with spherical or ellipsoidal shape and uniform dispersion. The SLN, FA-SLN and cRGD-FA-SLN particles were much larger than blank LN, indicating their successful modification with PEG and cRGD (Figure 4B).

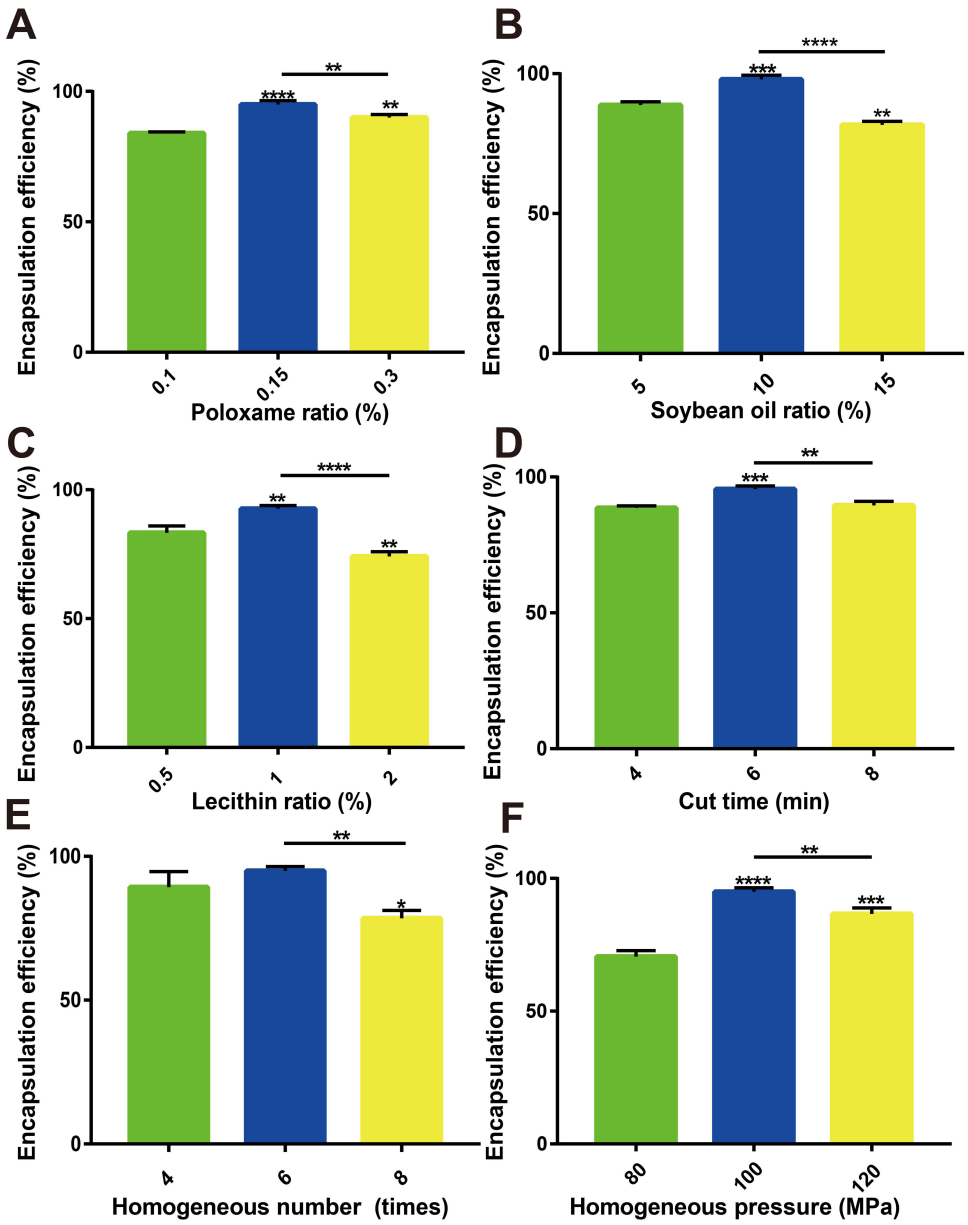

Figure 1 Results of single-factor screening. (**A**) poloxamer ratio, (**B**) soybean oil ratio, (**C**) lecithin ratio, (**D**) cut time, (**E**) homogeneous number and (**F**) homogeneous pressure on encapsulation efficiency of FA-SLN. Data are shown as mean ± SD (n = 3). $^{**}P < 0.01$, $^{***}P < 0.001$, $^{****}P < 0.0001$.

HPLC was performed to determine the EE values of the formulations (Table S4). The HPLC standard curve was linear within the range of 5.00 mg/L - 300.00 mg/L, and an intra- and inter-day relative standard deviation (RSD) of 2% was detected for these samples. Moreover, the blank recoveries of FA at low, medium, and high concentration levels were 101.60% (RSD, 0.56%), 101.6% (RSD, 1.60%), and 100.91% (RSD, 1.37%), respectively, indicating the reliability of the analytical method for measuring EE. The EE of the formulations used in the subsequent experiments were presented in Table S4.

The stability of FA-SLN and cRGD-FA-SLN was assessed at 4 °C and 30 °C. The appearance of both formulations, which was relatively uniform and milky-white with no oil droplets, remained unchanged after 10 days at 4 °C. Particle size, PDI, and K_e changed negligibly during this incubation, suggesting that FA-SLN and cRGD-FA-SLN are relatively stable at 4 °C (Table S5). In addition, FA-SLN showed good stability at 4 °C for three months. cRGD-FA-SLN also remained stable for one month, but oil droplet precipitation and stratification were observed after the second month, suggesting that the developed drug delivery system can be preserved at low temperatures for a limited time (Table S6). In contrast, storage of these two formulations at 30 °C for 10

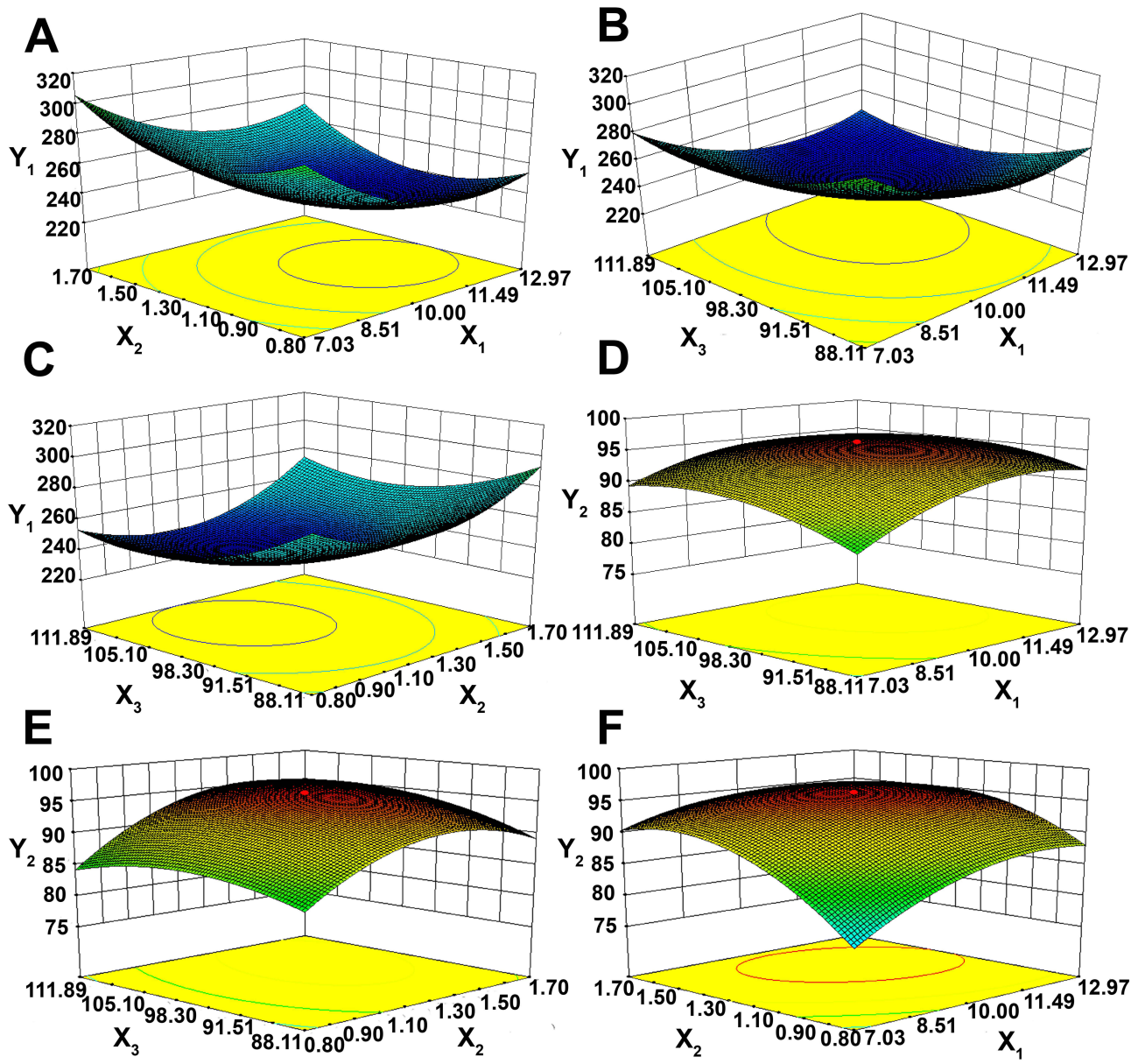

Figure 2 Effects of variables X_1 and X_2, and X_3. (**A**–**C**) particle size (Y_1) and (**D**–**F**) encapsulation efficiency (Y_2) of stealth lipid nanospheres loaded with flurbiprofen axetil (FA-SLN), as determined by the center composite design method. X_1, soybean oil ratio (%); X_2, lecithin ratio (%); X_3, homogeneous pressure (MPa).

days resulted in an uneven appearance with a small number of oil droplets after five days, whose number increased after another five days. Significant changes were also observed in the particle size, PDI, and K_e of both formulations (Table S7), indicating their instability under these conditions.

cRGD Enhancing the Uptake of LN Formulations by Activated Macrophages

The uptake of FA-LN, FA-SLN, and cRGD-FA-SLN by quiescent and LPS-activated macrophages was examined by confocal microscopy (Figure 5A). The number of M1-type RAW264.7 cells were considerably reduced in all treatment groups, probably due to some cell death during stimulation. The uptake of FA-LN by quiescent macrophages was higher than uptake of FA-SLN or cRGD-FA-SLN, reflecting the stealth function of PEG chains, which help evade detection and uptake by macrophages. In contrast, cRGD-FA-SLN showed the highest uptake by M1-type cells among all treatment groups, probably due to the overexpression of $\alpha_v\beta_3$ receptors on the cell surface, which can be selectively recognized by cRGD.[43] Flow cytometry confirmed that cRGD enhanced the uptake of LN formulations by activated macrophages (Figure 5B).

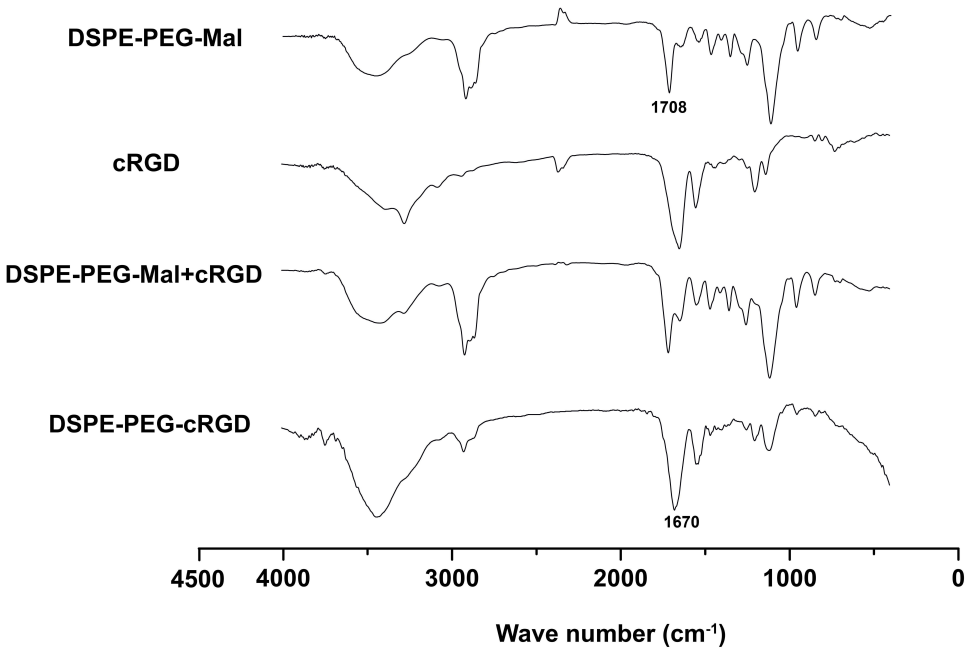

Figure 3 Fourier-transform infrared spectra of various formulations. DSPE-PEG-Mal+cRGD, the physical mixture of DSPE-PEG-Mal and cRGD.
Abbreviations: cRGD, cyclic arginine-glycine-aspartic acid peptide; DSPE, distearoyl phosphatidyl ethanolamine; Mal, maleimide; PEG, polyethylene glycol.

cRGD-FA-SLN Prolonging the Drug Circulating Time

The pharmacokinetic properties of FA were determined by measuring the content of its metabolite flurbiprofen in the blood samples of the CIA rats treated with different LN formulations (Figure 6). The concentration of flurbiprofen in the FA group reached a maximum level at around 6 min, while the concentration peak in the FA-LN group was detected at around 12 min. In contrast, the concentration of flurbiprofen in the FA-SLN and cRGD-FA-SLN groups peaked at 30 min, suggesting that the PEG modification can greatly retard drug release. Moreover, no significant differences were observed between FA-SLN and cRGD-FA-SLN groups or between healthy and CIA rats, indicating that neither cRGD nor the CIA procedure affected the metabolism of the drug in vivo.

Half-life ($T_{1/2z}$), area under the concentration-time curve (AUC), and mean residence time (MRT_{0-t}) were significantly better in the FA-LN group than in the FA group, in the case of healthy and CIA rats (Tables S8 and S9). These results confirm that the encapsulation of the drug into LNs can significantly prolong its circulation in vivo. Moreover, the half-life of the drug was significantly higher in the FA-SLN group than in the FA-LN group, suggesting that PEG modification further prolonged the drug in circulation. In contrast, no significant differences were detected between the cRGD-FA-SLN and FA-SLN groups, suggesting that cRGD does not affect drug circulation.

Results of Safety Assessment

The cytotoxicity of FA, SLN, FA-LN, FA-SLN, and cRGD-FA-SLN was examined in RAW264.7 cells (Figure 7). Treatment at various concentrations for 24, 48, and 72 h indicated that the cytotoxicity of cRGD-FA-SLN at 24 h was significantly lower than that of free FA when the concentration was above 60 μg/mL (Figure 7A). Significant differences were observed between the two groups of cRGD-FA-SLN and FA even at lower concentrations at 48 and 72 h after treatment (Figure 7B and C), suggesting that the encapsulation of FA into LNs can significantly reduce its toxicity. The effect of cRGD-FA-SLN on cell survival was also weaker than that of FA-LN, suggesting that the PEG chains helped avoid phagocytosis by macrophages. Cell survival was not significantly different after treatment with cRGD-FA-SLN or FA-SLN, indicating that RGD was not cytotoxic. Moreover, SLN, FA-LN, and FA-SLN were less cytotoxic than free FA, but no significant differences were

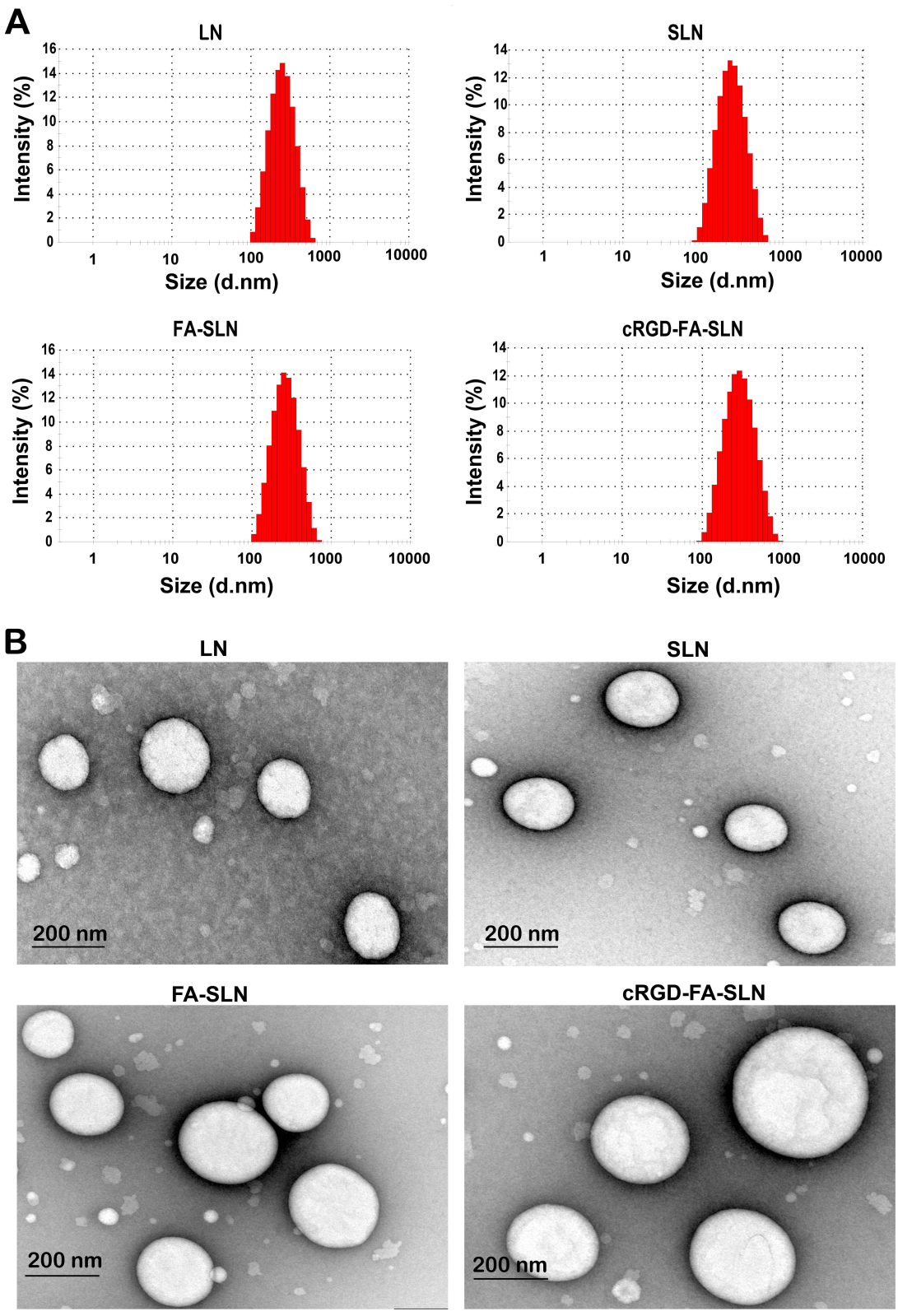

Figure 4 Particle size and morphology detection. (**A**) Particle size distribution and (**B**) transmission electron micrographs of LN, SLN, FA-SLN, and cRGD-FA-SLN. The bar is 100 nm.
Abbreviations: cRGD, cyclic arginine-glycine-aspartic acid peptide; FA, flurbiprofen axetil; LN, lipid nanospheres; SLN, stealth LN.

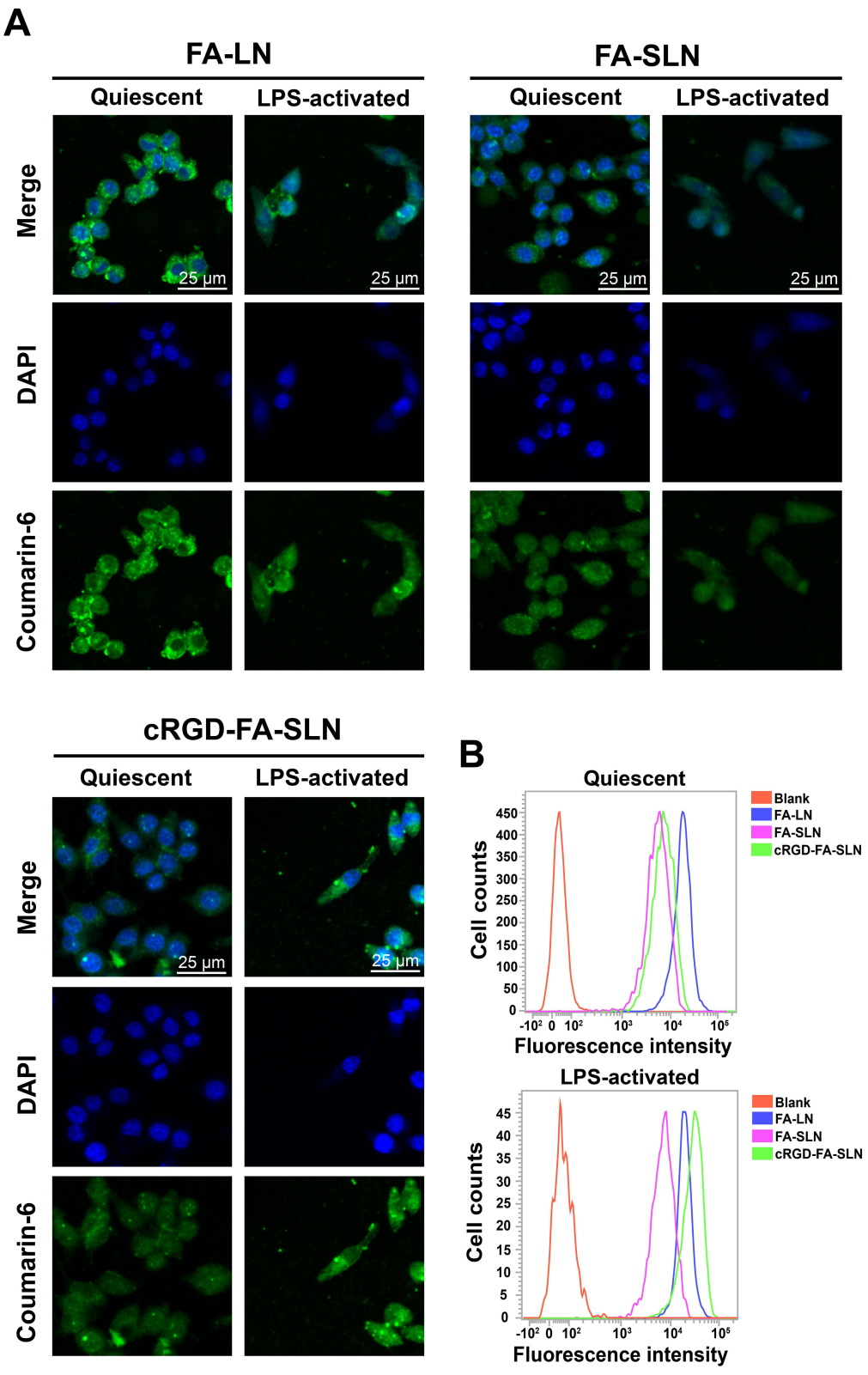

Figure 5 Cellular uptake detection. (**A**) Cellular uptake of FA-LN, FA-SLN, and cRGD-FA-SLN by quiescent and lipopolysaccharide-activated RAW264.7 macrophages (M1 type), as determined by confocal laser microscopy. (**B**) Frequency distributions of quiescent and M1-type RAW264.7 cells treated with different formulations.
Abbreviations: cRGD, cyclic arginine-glycine-aspartic acid peptide; DAPI, 4',6-diamidino-2-phenylin-dole dihydrochloride; FA, flurbiprofen axetil; LN, lipid nanospheres; SLN, stealth LN.

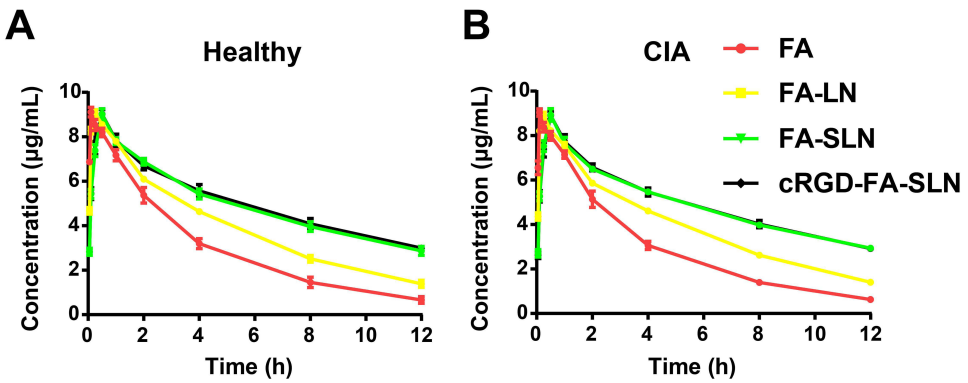

Figure 6 Pharmacokinetics of cRGD-FA-SLN in vivo. Changes in the concentration of flurbiprofen in the plasma from (**A**) the healthy and (**B**) collagen-induced arthritic (CIA) rats treated with FA, FA-LN, FA-SLN, or cRGD-FA-SLN. Data are shown as mean ± SD (n = 5).

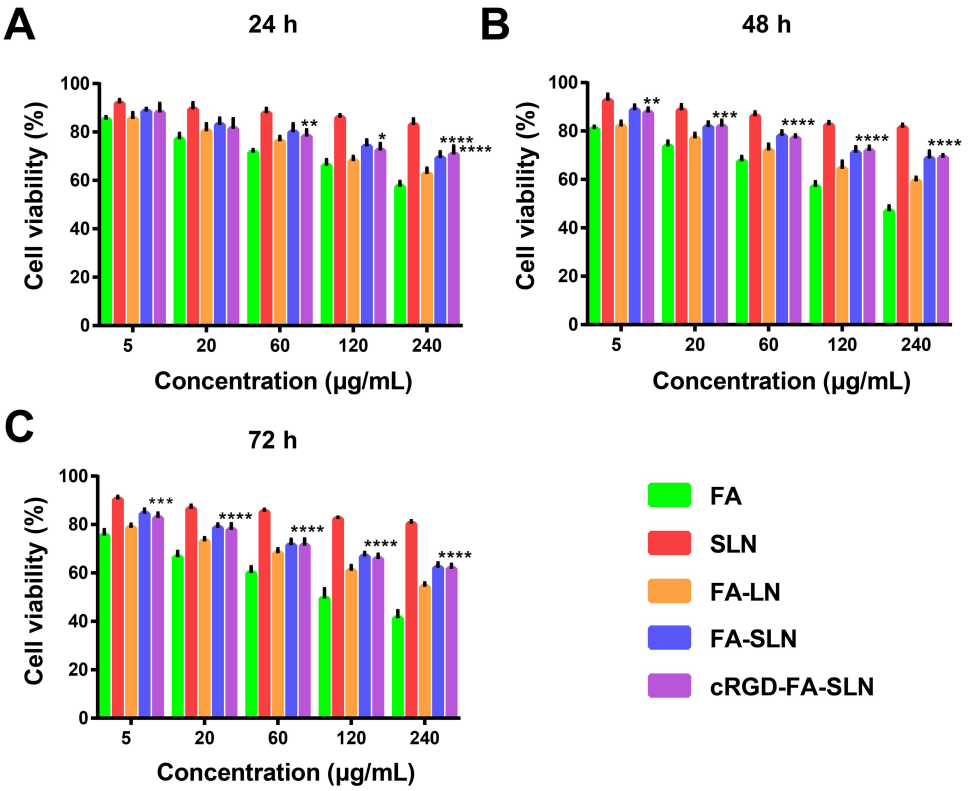

Figure 7 Effect of different formulations on RAW264.7 cell survival. (**A**) 24 h, (**B**) 48 h, and (**C**) 72 h post-administration, as determined by the MTT assay. Data are shown as mean ± SD (n = 3). *P < 0.05, **P < 0.01, ***P < 0.001, ****P < 0.0001 vs FA.

detected among these groups. Nevertheless, the cytotoxicity of all formulations increased with increasing concentration and time after administration.

The hemolytic potential of the prepared formulations in vitro increased with increasing concentration, but never exceeded 5% (Figure S3), suggesting their safety in vivo.

cRGD-FA-SLN Promoting the Inflammation-Targeting for the RA Treatment

In order to assess the inflammation-targeting ability of the prepared formulations, we examined the concentration of flurbiprofen in major organs collected from healthy and CIA rats at different time points after administration (Figure 8). Except for accumulation in joints, the biodistribution of the various preparations did not differ significantly between CIA

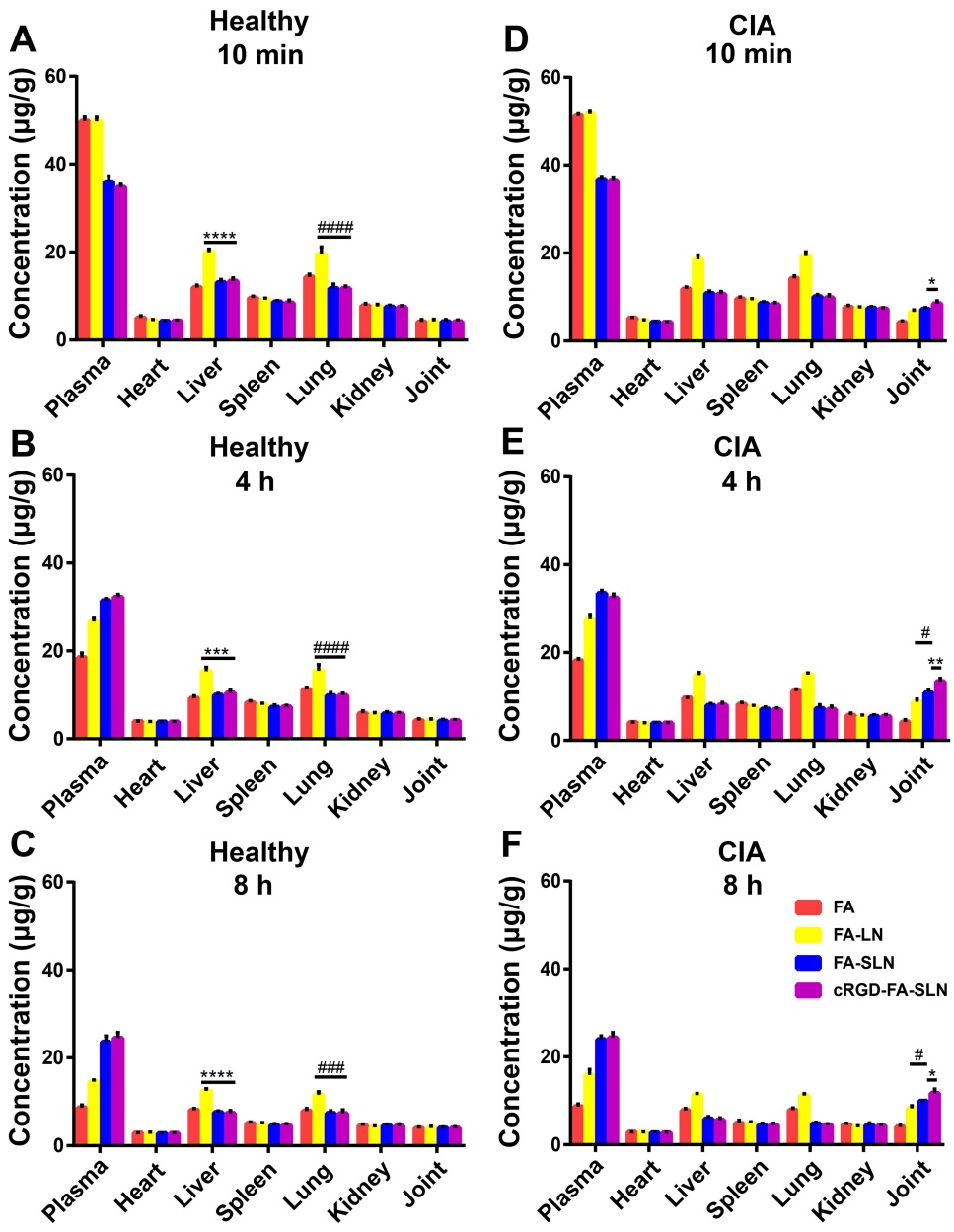

Figure 8 Biodistribution of different preparations in the tissues based on determination of flurbiprofen concentration. (**A**–**C**) Healthy and (**D**–**F**) collagen-induced arthritic (CIA) rats at 10 min, 4 h, and 8 h post-injection. Data are shown as mean ± SD (n = 5). *$P < 0.05$, **$P < 0.01$, ***$P < 0.001$, ****$P < 0.0001$; $^{\#}P < 0.05$, $^{\#\#\#}P < 0.001$, $^{\#\#\#\#}P < 0.0001$.

and healthy rats. In healthy rats (Figure 8A–C), the concentration of cRGD-FA-SLN in the liver and lungs was significantly lower than that of FA-LN, reflecting the strong RES in these organs. Moreover, the concentration of FA-SLN in the joints of CIA rats was significantly higher than that of FA-LN, but significantly lower than that of cRGD-FA-SLN (Figure 8D–F), confirming that cRGD enhances inflammation targeting.

Additional fluorescence measurements showed that FA-LN, FA-SLN, and cRGD-FA-SLN accumulated mainly in the inflamed joints of CIA rats, whereas free DiR was detected mainly in the lungs (Figure 9A). The fluorescence intensity of FA-LN, FA-SLN, and cRGD-FA-SLN in the ankle joints of healthy rats did not differ significantly from that of free DiR (Figure 9B). In contrast, the fluorescence signal of cRGD-FA-SLN in inflamed joints was significantly stronger than that of FA-SLN and FA-LN (Figure 9C and E). Ex vivo experiments confirmed that FA-LN accumulated mainly in the liver and lungs of healthy and CIA rats (Figure 9D).

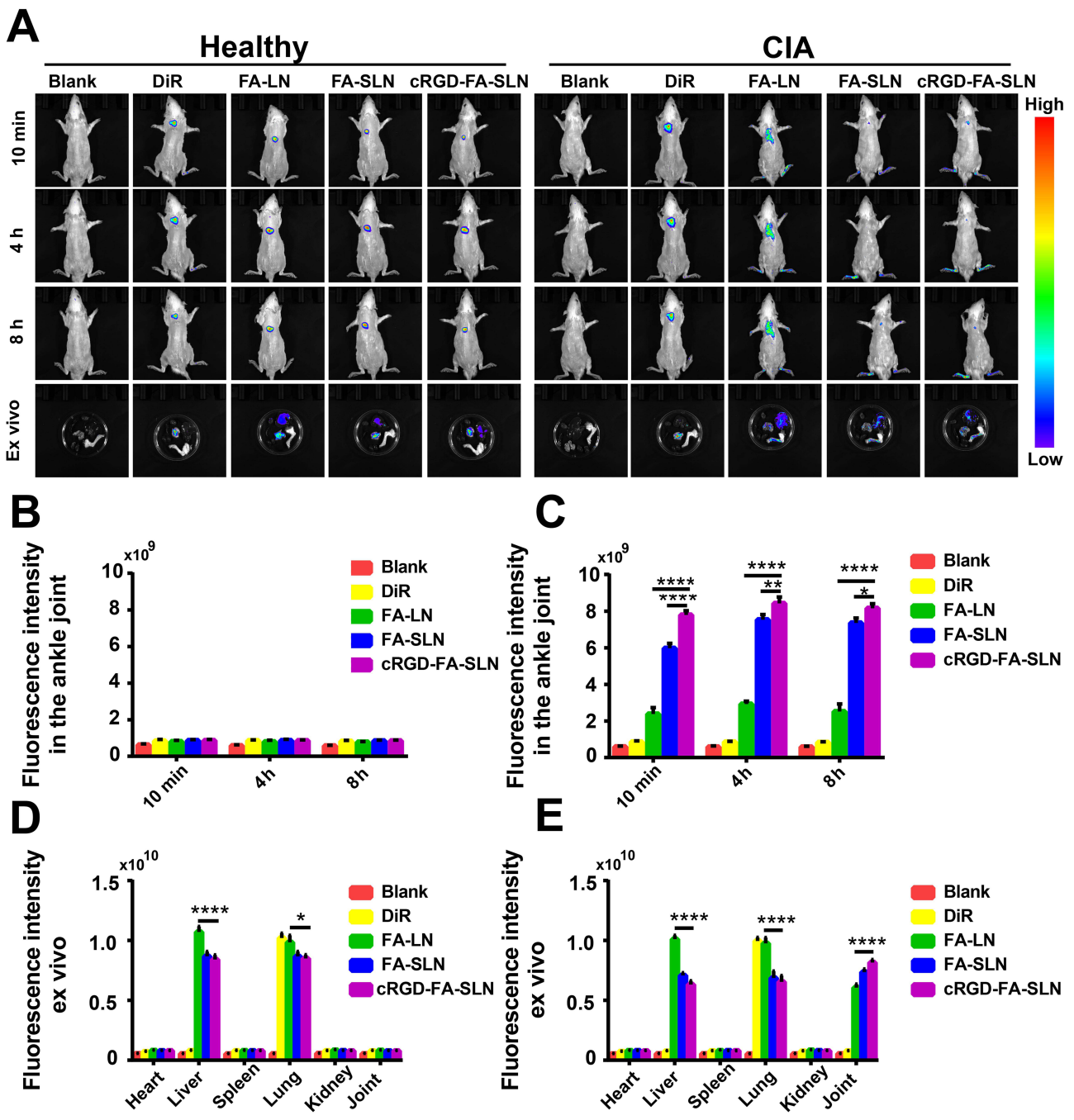

Figure 9 Biodistribution detection through the fluorescence measurements. (**A**) Biodistribution of DiR-labeled formulations in the tissues of healthy and collagen-induced arthritic (CIA) rats at 10 min, 4 h, and 8 h post-injection, as determined by in vivo fluorescence imaging. (**B**–**E**) Semi-quantitative analysis of fluorescence intensity in (**B**) healthy ankle joints, (**C**) inflamed ankle joints, (**D**) tissues of healthy rats, and (**E**) tissues of CIA rats. Data are shown as mean ± SD (n = 5). **P* < 0.05, ***P* < 0.01, *****P* < 0.0001. DiR, 1.1-dioctadecyl-3,3,3,3-tetramethylindotricarbocyanine.

Taken together, these results suggest that modification with cRGD and PEG can strongly improve the ability of LNs to target inflammation sites in vivo and reduce their clearance by RES in the liver and lungs.

cRGD-FA-SLN Enhancing the in vivo Therapeutic Efficacy of RA

On day 34 after CIA induction, the swelling of hind legs (Figure 10A), body weight (Figure 10B), ankle diameter (Figure 10C), paw volume (Figure 10D), and AI score (Figure 10E) were significantly lower in animals treated with FA-

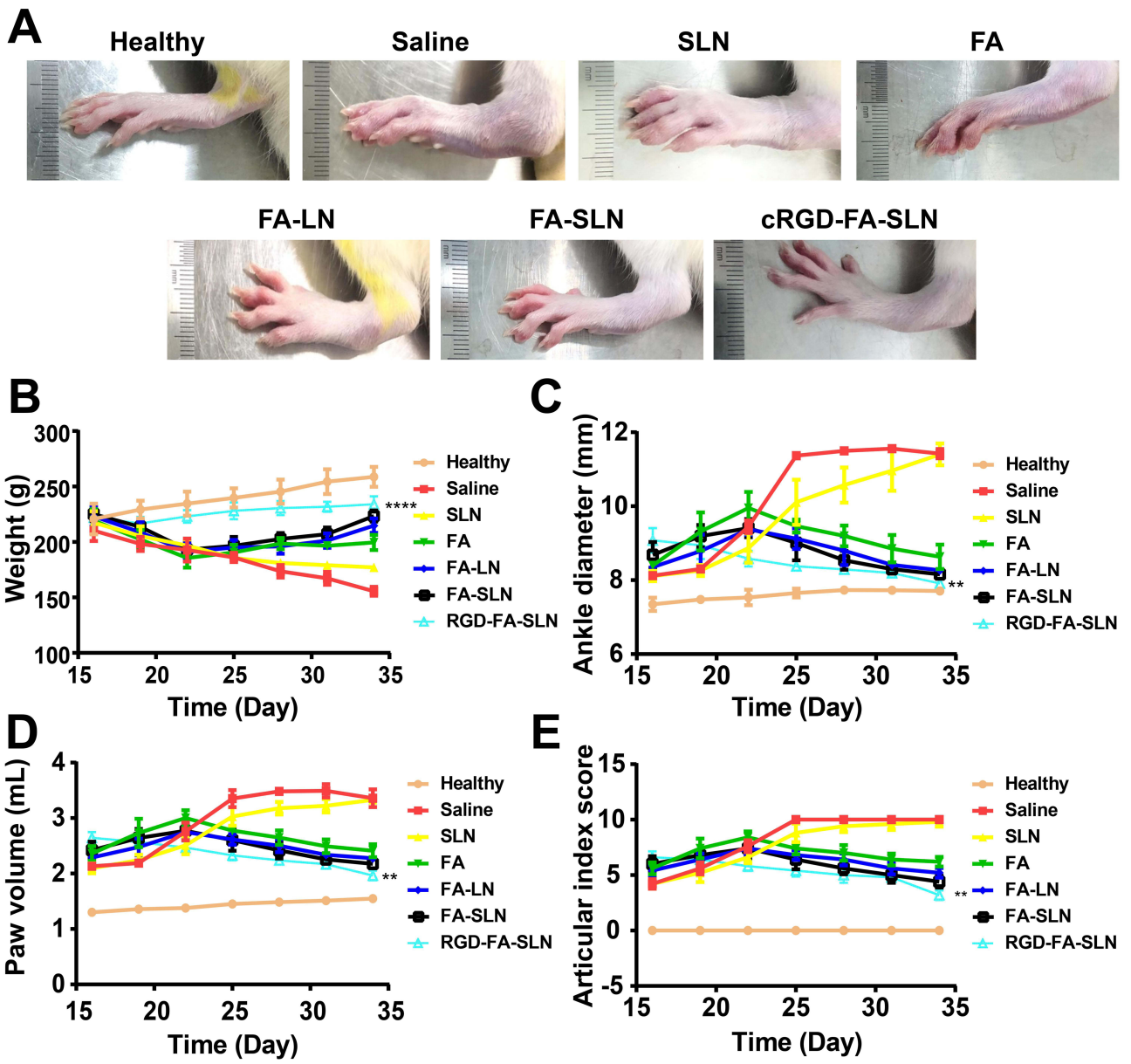

Figure 10 In vivo therapeutic efficacy of cRGD-FA-SLN. (**A**) Photographs of hind legs collected from rats in different treatment groups on day 34 after arthritis induction. (**B**–**E**) Changes in the (**B**) weight, (**C**) ankle diameter, (**D**) paw volume, and (**E**) articular index score over time. Data are shown as mean ± SD (n = 5). $^{**}P < 0.01$, $^{****}P < 0.0001$ vs saline.

LN or cRGD-FA-SLN than in animals treated with saline, SLN, or free FA. This result suggests that the developed formulations can effectively delay arthritis progression.

The beneficial effects of the developed platform were also observed by high-resolution micro-CT (Figure 11A). cRGD-FA-SLN significantly reduced the effects of CIA on the quality of ankle joint bones compared to saline or SLN. Their effects were also significantly better than those of free FA and FA-SLN (Figure 11B–G), suggesting that cRGD-FA-SLN may help rebuild the bone microarchitecture in CIA rats.

Next, we examined the histopathological changes in ankle joint tissues. Hematoxylin-eosin (H&E) staining revealed a clear, intact synovial structure with a small amount of fibrous tissue hyperplasia in the cRGD-FA-SLN group, whereas such fibrosis was not observed in healthy controls. In contrast, the bone tissue in the saline and SLN groups was severely damaged and the bone structure was incomplete. More specifically, the cartilage and subchondral bone tissue were eroded, the cartilage layer was thinned, some bone trabeculae were necrotic, the number of osteoclasts in the necrotic

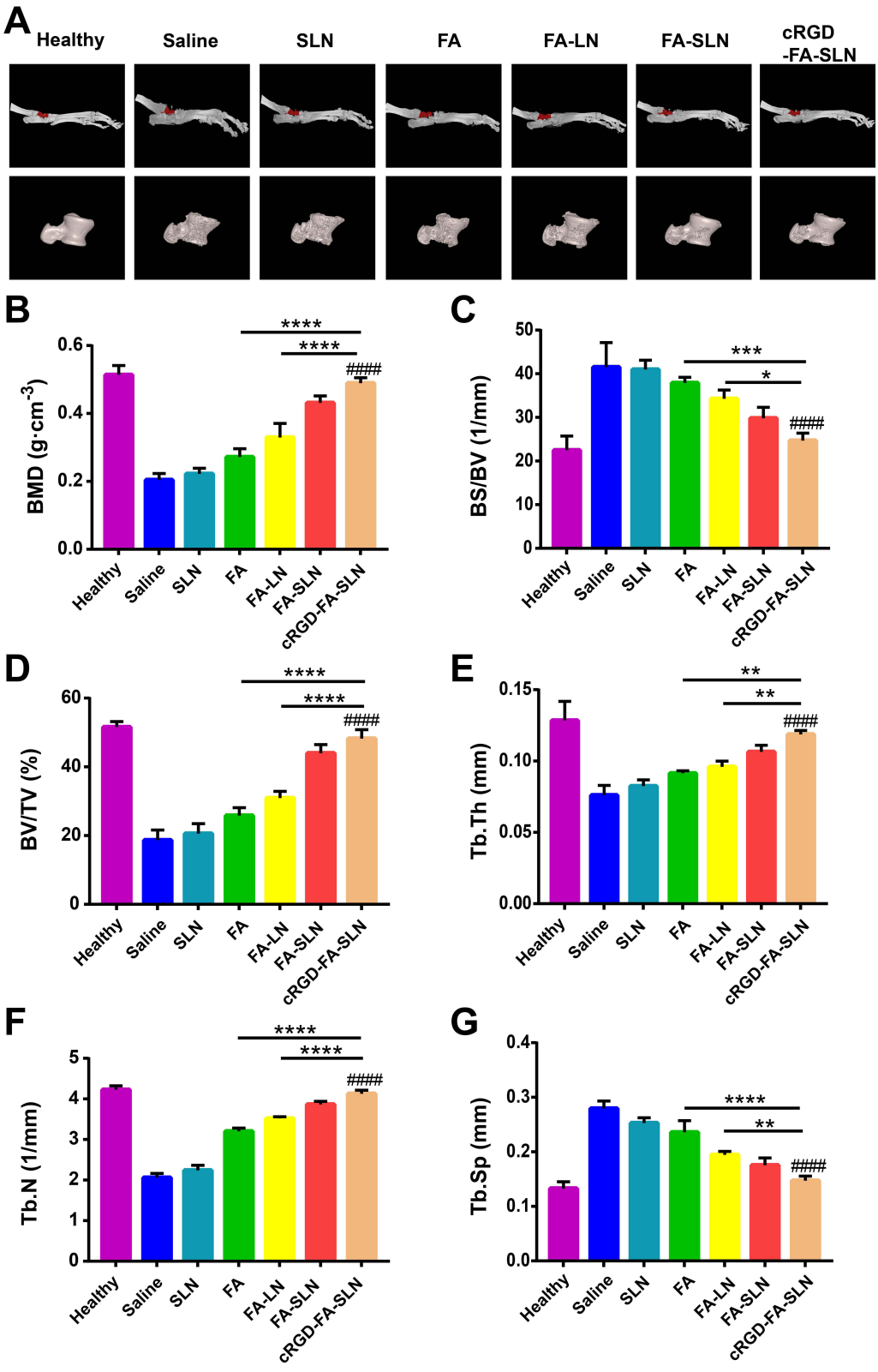

Figure 11 Micro-computed tomography detection of ankle joints. (**A**) Three-dimensional micro-computed tomography images of ankle joint bones. (**B**–**G**) Effect of different treatments on (**B**) bone mineral density (BMD), (**C**) ratio of bone surface area to bone volume (BS/BV), (**D**) ratio of bone volume to tissue volume (BV/TV), (**E**) trabecular thickness (Tb.Th), (**F**) trabecular number (Tb.N), (**G**) and trabecular spacing (Tb.Sp). Data are shown as mean ± SD (n = 5). $^{\#\#\#\#}P < 0.0001$ vs saline; $^{*}P < 0.05$, $^{**}P < 0.01$, $^{***}P < 0.001$, $^{****}P < 0.0001$.

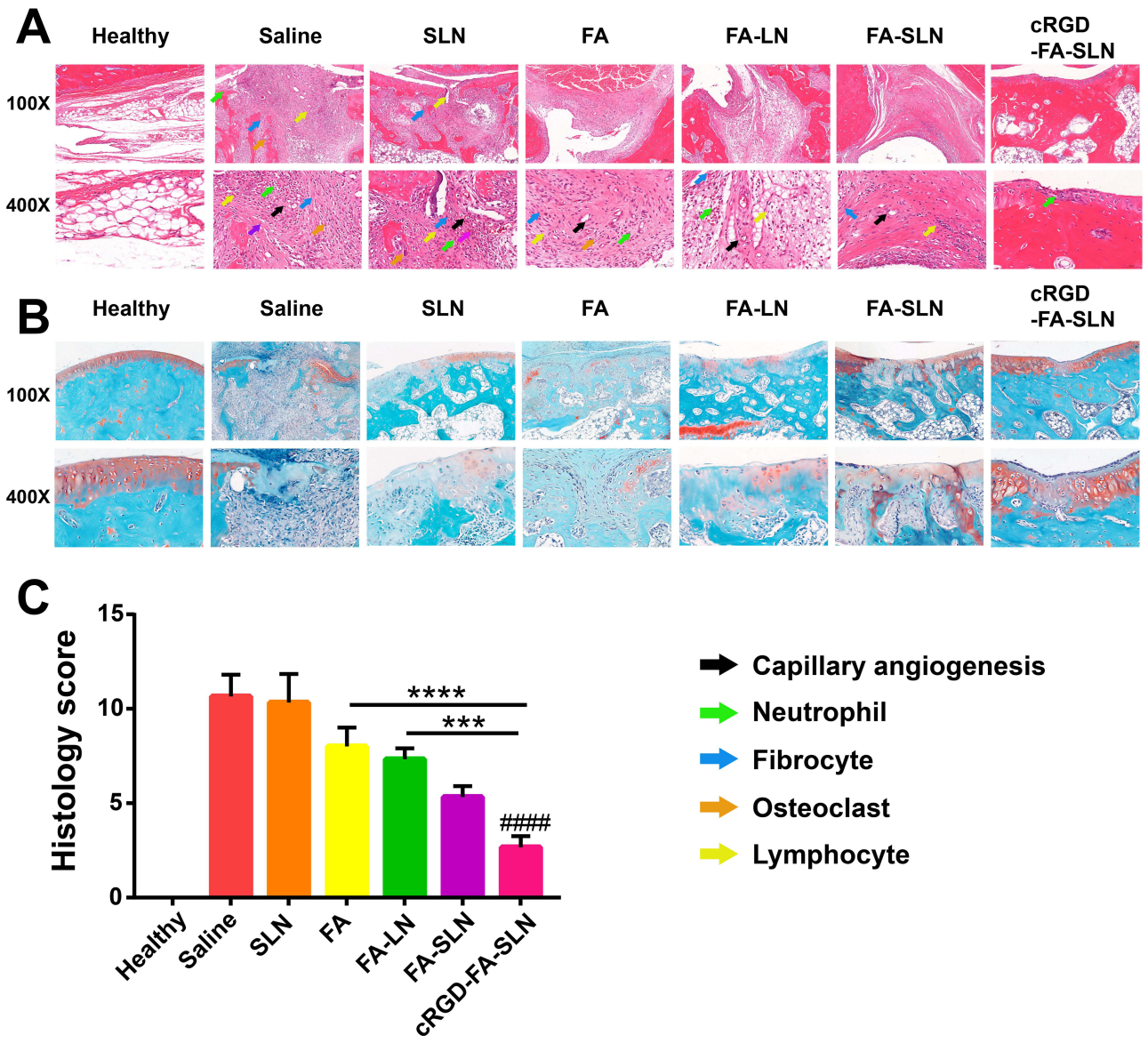

Figure 12 Histopathological changes in ankle joint tissues. (**A**) Hematoxylin–eosin and (**B**) safranin O staining of ankle joint tissues collected from rats after various treatments. (**C**) Histopathological scores in the different treatment groups. Data are shown as mean ± SD (n = 5). $^{\#\#\#\#}P < 0.0001$ vs saline. $^{***}P < 0.001$, $^{****}P < 0.0001$ (cRGD-FA-SLN vs FA or FA-LN).

area was increased, a large amount of fibrous tissue proliferated, and new capillaries had formed. FA, FA-LN, and FA-SLN moderately affected disease progression (Figure 12A).

The cRGD-FA-SLN group also showed uniform articular cartilage thickness and complete tide line, similar to healthy animals; whereas animals treated with saline or SLN showed varying cartilage thickness and incomplete tide line. In addition, FA, FA-LN, and FA-SLN were less effective than cRGD-FA-SLN in mitigating articular cartilage injury (Figure 12B and C).

The pain threshold of CIA rats was also assessed to determine the analgesic effect of the prepared formulations (Table S10), based on the idea that paws should be more sensitive to high temperatures in the presence of inflammation. Rats were placed on a plate preheated at 55 °C. At 15 min, the pain threshold was significantly higher in both FA-SLN and cRGD-FA-SLN groups than that in the saline group. In addition, the pain threshold was significantly higher in the cRGD-FA-SLN group than that in the other treatment groups at all time points, confirming the high targeting efficiency endowed by cRGD. Interestingly, the pain

thresholds of the FA-SLN and cRGD-FA-SLN groups did not change significantly over time, confirming that the modification with PEG prolongs drug action.

The analgesic effect was further evaluated by injecting rats with acetic acid to induce a torsional response (Table S11). The number of torsions was considerably reduced after treatment with FA-SLN and cRGD-FA-SLN compared to saline, but no significant difference was observed between FA-SLN and cRGD-FA-SLN, as the torsional response induced by acetic acid was a generalized pain, not directly associated with the foot joint.

Furthermore, cRGD-FA-SLN reduced the coefficient of spleen and thymus (Figure 13A and B) and PGE2 (Figure 13E) to normal levels, suggesting that the encapsulation of FA into LNs improved its therapeutic efficacy against RA. Meanwhile, the platform significantly reduced the serum levels of alanine aminotransferase (ALT)

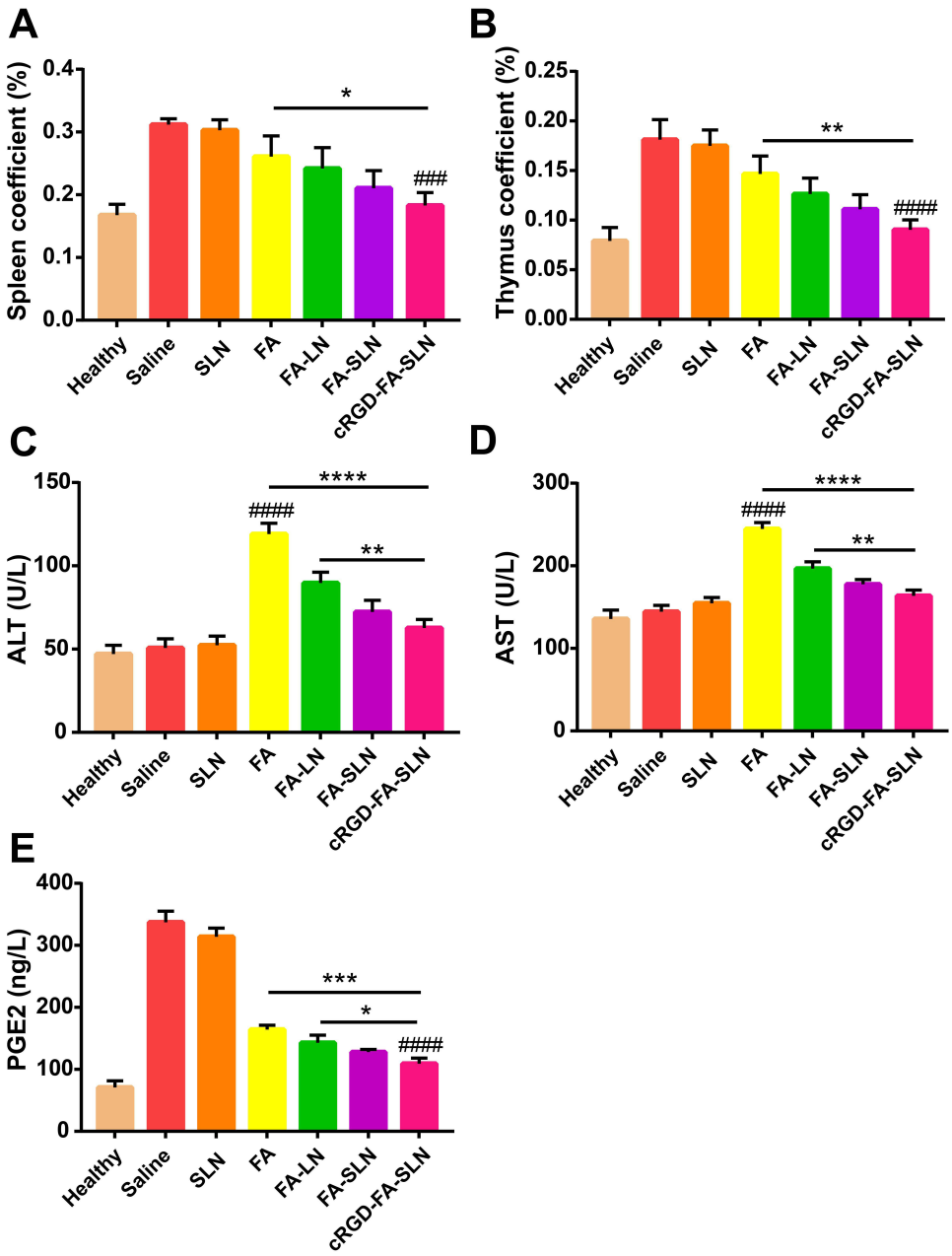

Figure 13 Effect of the different treatments on the (**A**) spleen coefficient, (**B**) thymus coefficient, as well as levels of (**C**) alanine aminotransferase (ALT), (**D**) aspartate aminotransferase (AST), and (**E**) prostaglandin E2 (PGE2). Data are shown as mean ± SD (n = 3). $^{\#\#\#\#}P < 0.001$, $^{\#\#\#\#\#}P < 0.0001$ vs saline; $^{*}P < 0.05$, $^{**}P < 0.01$, $^{***}P < 0.001$, $^{****}P < 0.0001$.

and aspartate aminotransferase (AST) in CIA rats (Figure 13C and D), indicating that the encapsulation of FA into LNs effectively reduced the hepatotoxicity of the drug.

Discussion

In this study, LNs modified with PEG and the cRGD peptide were loaded with FA to prepare a drug delivery platform for targeted RA treatment. The formulation was optimized by single-factor screening and CCD. cRGD-FA-SLN showed good encapsulation efficiency for FA and was effectively taken up in vitro by activated macrophages. In vivo and ex vivo experiments showed that cRGD-FA-SLN distributed mainly to arthritic ankle joints, showing good analgesic effects and less hepatotoxicity than the free drug.

The particle size of cRGD-FA-SLN was less than 300 nm and PDI was below 0.3, indicating that the LNs can pass easily through the capillaries and be uniformly dispersed without causing blockage.[44] Although the zeta potential was close to zero, cRGD-FA-SLN proved to be stable at 4 °C, suggesting that the surface charge does not affect the stability of the formulation.

DSPE-PEG_{2000} is widely used in long-cycle formulations.[45] Moreover, the short cRGD peptide is known for its high stability and low immunogenicity.[46] Therefore, we considered that modifying FA-loaded LNs with cRGD and PEG would significantly improve their properties. Indeed, we found that cRGD-FA-SLN can successfully avoid RES clearance and enhance the inflammation-targeting ability of FA-SLN, while reducing the required drug dosage. In addition, the cytotoxicity of free FA was significantly reduced after encapsulation into cRGD-FA-SLN, confirming the safety of the developed platform for in vivo applications.

Macrophages play a key role in the onset and development of RA. Under external stimulation, macrophages differentiate into (i) M1-type cells, which secrete pro-inflammatory factors and are overexpressed in RA, and (ii) M2-type cells, which secrete mainly anti-inflammatory factors.[18] Here, we found that cRGD-FA-SLN were preferentially internalized by activated M1-macrophages, suggesting that this delivery system can escape elimination by normal macrophages in the RES, thereby promoting the accumulation of the drug at the inflamed arthritic site and enhancing its therapeutic efficacy.

Consistent with a previous study,[47] the peak time of the FA-LN group was determined at around 10 min with a half-life of about 4 h. Thus, the distribution of the prepared formulation in various tissues was determined at 10 min, 4 h, and 8 h, when drug metabolism was more intense.

Tissue distribution shows that in the ankle joint of the healthy rats the higher accumulation of FA-SLN almost equivalent to cRGD-FA-SLN. It may be due to the fact that macrophages in the healthy rats are not polarized by inflammation, their surface does not overexpress αvβ3 receptors. Therefore, the cRGD in cRGD-FA-SLN did not produce active targeting effects in healthy rats. The higher accumulation of FA-SLN almost equivalent to cRGD-FA-SLN in the healthy ankle joints. However, in the ankle joints of CIA model rats, the concentration levels of cRGD-FA-SLN and FA-SLN were significantly different.

Leg bones were scanned by micro-CT to visualize the three-dimensional structure. In addition, sections were stained with H&E and Safranin O. The results showed that long-circulating, PEG-modified LNs were more effective than regular LNs. Compared to the other treatment groups, cRGD-FA-SLN more effectively targeted sites of inflammation and delayed disease progression in vivo, while prolonging drug efficacy and reducing FA toxicity.

Although our study suggests the efficacy of cRGD-FA-SLN for RA treatment, the clinical suitability of such drug delivery systems depends on numerous factors, such as the time of application during the disease course. These factors require further investigation. In addition, the CIA rat model may not fully recapitulate the development of RA. Therefore, future studies should aim to explore RA pathology in greater detail, particularly processes occurring early in the disease course.

Conclusions

cRGD-FA-SLN was constructed as a novel drug delivery system for the targeted treatment of RA. The developed platform was able to avoid clearance by the RES in vivo and actively target inflammation sites by binding to the $\alpha_v\beta_3$ receptor, while it showed lower cytotoxicity and longer circulation time than the free drug. cRGD-FA-SLN will serve as

a promising platform for the delivery of NSAIDs and will pave the way for the development of novel agents for the clinical treatment of RA.

Abbreviations

ALT, aspartate aminotransferase; AST, Alanine aminotransferase; CIA, collagen-induced arthritis; CCD, central composite design; cRGD-FA-SLM, cRGD mediated stealth lipid microsphere loaded with flurbiprofen axetil; DMEM, dulbecco's modified eagle media; DMSO, dimethyl sulfoxide; EPR, enhanced permeability and retention effect; EE, encapsulation efficiency; ELISA, enzyme linked immunosorbent assay; FA, flurbiprofen axetil; FP, flurbiprofen; FTIR, Fourier transform infrared spectroscopy; HPLC, high-performance liquid chromatography; LM, lipid microsphere; LPS, lipopolysaccharide; NSAIDs, non-steroid anti-inflammatory drug; PDI, polydispersity index; PGE2, prostaglandin E2; RA, rheumatoid arthritis; RES, reticuloendothelial system; SLM, stealth lipid microsphere; TEM, transmission electron microscope.

Data Sharing Statement

Data will be made available on request.

Acknowledgments

This work was supported by grants from the Sichuan Science and Technology Program (2022YFS0188, 2022YFS0627), the Cooperative Scientific Research Project of Chunhui Plan of the Ministry of Education of China (202200618), Science and Technology Project of Luzhou Government (2021-SYF-33, 2020-JYJ-47, 2022SWMU4), Central Nervous System Drug Key Laboratory of Sichuan Province (210020-01SZ).

Disclosure

The authors declare that they have no known competing financial interests or personal relationships that could have appeared to influence the work reported in this paper.

References

1. Ptacek J, Hawtin RE, Sun D, et al. Diminished cytokine-induced Jak/STAT signaling is associated with rheumatoid arthritis and disease activity. *PLoS One*. 2021;16:1. doi:10.1371/journal.pone.0244187
2. Tanaka Y, Hoshino-Negishi K, Kuboi Y, et al. Emerging role of fractalkine in the treatment of rheumatic diseases. *Immunotargets Ther*. 2020;9:241–253. doi:10.2147/itt.S277991
3. Ye Z, Shen Y, Jin K, et al. Arachidonic acid-regulated calcium signaling in T cells from patients with rheumatoid arthritis promotes synovial inflammation. *Nat Commun*. 2021;12(1):907. doi:10.1038/s41467-021-21242-z
4. Yang M, Feng X, Ding J, et al. Nanotherapeutics relieve rheumatoid arthritis. *J Control Release*. 2017;252:108–124. doi:10.1016/j.jconrel.2017.02.032
5. Gunasekera WM, Kirwan JR. Rheumatoid arthritis: previously untreated early disease. *BMJ Clin Evid*. 2016;2016:1.
6. Wei W, Lu W, Chen X, et al. Use of network pharmacology to investigate the mechanism of the compound xuanju capsule in the treatment of rheumatoid arthritis. *Biomed Res Int*. 2021;2021:1–14. doi:10.1155/2021/5568791
7. Feldmann M, Maini RN. Perspectives from masters in rheumatology and autoimmunity: can we get closer to a cure for rheumatoid arthritis? *Arthritis Rheumatol*. 2015;67(9):2283–2291. doi:10.1002/art.39269
8. Arfè A, Scotti L, Varas-Lorenzo C, et al. Non-steroidal anti-inflammatory drugs and risk of heart failure in four European countries: nested case-control study. *BMJ*. 2016;354. doi:10.1136/bmj.i4857
9. Qiu S, Wu X, Li Z, et al. A smart nanoreactor based on an O2-economized dual energy inhibition strategy armed with dual multi-stimuli-responsive "Doorkeepers" for Enhanced CDT/PTT of rheumatoid arthritis. *ACS Nano*. 2022;16(10):17062–17079. doi:10.1021/acsnano.2c07338
10. Qiu S, Wu X, Geng D, et al. H2O2/NIR-sensitive "two-step" nano theranostic system based hollow mesoporous copper sulfide/hyaluronic acid/JWH133 as an optimally designed delivery system for multidimensional treatment of RA. *Int J Biol Macromol*. 2023;225:298–309. doi:10.1016/j.ijbiomac.2022.11.019
11. Yuan F, Quan LD, Cui L, et al. Development of macromolecular prodrug for rheumatoid arthritis. *Adv Drug Deliv Rev*. 2012;64(12):1205–1219. doi:10.1016/j.addr.2012.03.006
12. Zhao M, Liu M. New avenues for nanoparticle-related therapies. *Nanoscale Res Lett*. 2018;13(1):136. doi:10.1186/s11671-018-2548-8
13. Zhou M, Hou J, Zhong Z, et al. Targeted delivery of hyaluronic acid-coated solid lipid nanoparticles for rheumatoid arthritis therapy. *Drug Deliv*. 2018;25(1):716–722. doi:10.1080/10717544.2018.1447050
14. Liu S. Radiolabeled multimeric cyclic RGD peptides as integrin alphavbeta3 targeted radiotracers for tumor imaging. *Mol Pharm*. 2006;3(5):472–487. doi:10.1021/mp060049x

15. Wilder RL. Integrin alpha V beta 3 as a target for treatment of rheumatoid arthritis and related rheumatic diseases. *Ann Rheum Dis*. 2002;61(2):96ii–99. doi:10.1136/ard.61.suppl_2.ii96
16. Liu W, Zhang Y, Zhu W, et al. Sinomenine inhibits the progression of rheumatoid arthritis by regulating the secretion of inflammatory cytokines and monocyte/macrophage subsets. *Front Immunol*. 2018;9:2228. doi:10.3389/fimmu.2018.02228
17. Emam SH, Sonousi A, Osman EO, et al. Design and synthesis of methoxyphenyl- and coumarin-based chalcone derivatives as anti-inflammatory agents by inhibition of NO production and down-regulation of NF-κB in LPS-induced RAW264.7 macrophage cells. *Bioorg Chem*. 2021;107:104630. doi:10.1016/j.bioorg.2021.104630
18. Matsumoto T, Takahashi N, Kojima T, et al. Soluble Siglec-9 suppresses arthritis in a collagen-induced arthritis mouse model and inhibits M1 activation of RAW264.7 macrophages. *Arthritis Res Ther*. 2016;18(1):133. doi:10.1186/s13075-016-1035-9
19. Fu S, Xu X, Ma Y, et al. RGD peptide-based non-viral gene delivery vectors targeting integrin α v β 3 for cancer therapy. *J Drug Target*. 2019;27(1):1–11. doi:10.1080/1061186x.2018.1455841
20. Lomen PL, Lamborn KR, Porter GH, et al. Treatment of osteoarthritis of the knee. A comparison of flurbiprofen and aspirin. *Am J Med*. 1986;80(3a):97–102. doi:10.1016/0002-9343(86)90122-1
21. Zhao X, Ji L. Flurbiprofen axetil: analgesic effect and adverse reaction. *Pak J Pharm Sci*. 2018;31:1163–1167.
22. Zhang J, Zhang H, Zhao L, Gu J, Feng Y, An H. Erratum: population pharmacokinetic modeling of flurbiprofen, the active metabolite of flurbiprofen Axetil, in Chinese Patients with Postoperative Pain. *J Pain Res*. 2020;13:553. doi:10.2147/jpr.S251590
23. Tyagi P, Santos JL. Macromolecule nanotherapeutics: approaches and challenges. *Drug Discov Today*. 2018;23(5):1053–1061. doi:10.1016/j.drudis.2018.01.017
24. Er Y, Barnes TJ, Fornasiero D, et al. The encapsulation and release of guanosine from PEGylated liposomes. *J Liposome Res*. 2009;19(1):29–36. doi:10.1080/08982100802673940
25. Saneja A, Kumar R, Singh A, et al. Development and evaluation of long-circulating nanoparticles loaded with betulinic acid for improved anti-tumor efficacy. *Int J Pharm*. 2017;531(1):153–166. doi:10.1016/j.ijpharm.2017.08.076
26. Usta A, Man KP, Strong N, et al. Investigating MTX-Loaded magnetic nanocomposite particles for treatment of rheumatoid arthritis. *J Magn Magn Mater*. 2020;499:166171. doi:10.1016/j.jmmm.2019.166171
27. Wu H, Su S, Wu Y, et al. Nanoparticle-facilitated delivery of BAFF-R siRNA for B cell intervention and rheumatoid arthritis therapy. *Int Immunopharmacol*. 2020;88:106933. doi:10.1016/j.intimp.2020.106933
28. Guo Y, Ye Q, Yang S, et al. Therapeutic effects of polysaccharides from Anoectochilus roxburghii on type II collagen-induced arthritis in rats. *Int J Biol Macromol*. 2019;122:882–892. doi:10.1016/j.ijbiomac.2018.11.015
29. Ma YX, Song YX, Ma F, et al. a potential polymeric nanogel system for effective delivery of chlorogenic acid to target collagen-induced arthritis. *J Inorg Organomet Polym Mater*. 2020;30(7):2356–2365. doi:10.1007/s10904-019-01421-8
30. Liang X, Chen X, Zhao G, et al. Preparation, characterization, and pharmacokinetic evaluation of imperatorin lipid microspheres and their effect on the proliferation of MDA-MB-231 Cells. *Pharmaceutics*. 2018;10(4):236. doi:10.3390/pharmaceutics10040236
31. Chen Z, Luo Z, Lyu J, et al. Preparation and formulation optimization of methotrexate-loaded human serum albumin nanoparticles modified by mannose. *Curr Med Chem*. 2021;28(24):5016–5029. doi:10.2174/0929867328666210118112640
32. Aktan B, Chambre L, Sanyal R, et al. "Clickable" nanogels via thermally driven self-assembly of polymers: facile access to targeted imaging platforms using thiol-maleimide conjugation. *Biomacromolecules*. 2017;18(2):490–497. doi:10.1021/acs.biomac.6b01576
33. Liu XY, Ruan LM, Mao WW, et al. Preparation of RGD-modified long circulating liposome loading matrine, and its in vitro anti-cancer effects. *Int J Med Sci*. 2010;7(4):197–208. doi:10.7150/ijms.7.197
34. Tizro P, Choi C, Khanlou N. sample preparation for transmission electron microscopy. *Methods Mol Biol*. 2019;1897:417–424. doi:10.1007/978-1-4939-8935-5_33
35. Huang X, Li Y, Fu M, Xin HB. Polarizing macrophages in vitro. *Methods Mol Biol*. 2018;1784:119–126. doi:10.1007/978-1-4939-7837-3_12
36. Hinz B, Brune K, Rau T, et al. Flurbiprofen enantiomers inhibit inducible nitric oxide synthase expression in RAW 264.7 macrophages. *Pharm Res*. 2001;18(2):151–156. doi:10.1023/a:1011020132140
37. Boutet MA, Najm A, Bart G, et al. IL-38 overexpression induces anti-inflammatory effects in mice arthritis models and in human macrophages in vitro. *Ann Rheum Dis*. 2017;76(7):1304–1312. doi:10.1136/annrheumdis-2016-210630
38. Wu J, Fan KJ, Wang QS, et al. DMY protects the knee joints of rats with collagen-induced arthritis by inhibition of NF-κB signaling and osteoclastic bone resorption. *Food Funct*. 2020;11(7):6251–6264. doi:10.1039/d0fo00396d
39. Wang Q, Jiang H, Li Y, et al. Targeting NF-kB signaling with polymeric hybrid micelles that co-deliver siRNA and dexamethasone for arthritis therapy. *Biomaterials*. 2017;122:10–22. doi:10.1016/j.biomaterials.2017.01.008
40. Kubota A, Suguro T, Nakajima A, et al. Effect of biological agents on synovial tissues from patients with rheumatoid arthritis. *Mod Rheumatol*. 2020;30(2):282–286. doi:10.1080/14397595.2019.1583783
41. Luo S, Li H, Liu J, et al. Andrographolide ameliorates oxidative stress, inflammation and histological outcome in complete Freund's adjuvant-induced arthritis. *Chem Biol Interact*. 2020;319:108984. doi:10.1016/j.cbi.2020.108984
42. Wang Y, Yan M, Zheng GY, et al. A cell-based, high-throughput homogeneous time-resolved fluorescence assay for the screening of potential κ-opioid receptor agonists. *Acta Pharmacol Sin*. 2014;35(7):957–966. doi:10.1038/aps.2014.21
43. Deng C, Zhang Q, He P, et al. Targeted apoptosis of macrophages and osteoclasts in arthritic joints is effective against advanced inflammatory arthritis. *Nat Commun*. 2021;12(1):2174. doi:10.1038/s41467-021-22454-z
44. Maître JM, Boss G, Testa B. High-performance liquid chromatographic separation of the enantiomers of anti-inflammatory 2-arylpropionates: suitability of the method for in vitro metabolic studies. *J Chromatogr*. 1984;299(2):397–403. doi:10.1016/s0021-9673(01)97855-0
45. Huckaby JT, Jacobs TM, Li Z, et al. Structure of an anti-PEG antibody reveals an open ring that captures highly flexible PEG polymers. *Commun Chem*. 2020;3(1):124. doi:10.1038/s42004-020-00369-y
46. Sun Y, Kang C, Liu F, et al. RGD peptide-based target drug delivery of doxorubicin nanomedicine. *Drug Dev Res*. 2017;78(6):283–291. doi:10.1002/ddr.21399
47. Davies NM. Clinical pharmacokinetics of flurbiprofen and its enantiomers. *Clin Pharmacokinet*. 1995;28(2):100–114. doi:10.2165/00003088-199528020-00002